SERVICE LIFE PREDICTION OF REINFORCED CONCRETE BRIDGE DECK

by

Alaa Binmerdah

Submitted in partial fulfillment of the requirements
for the Master of Applied Science

at

Dalhousie University
Halifax, Nova Scotia
September 2018

TABLE OF CONTENTS

LIST OF TABLES

LIST OF FIGURES

ABSTRACT

Chloride ions are a major cause of deterioration for reinforced concrete structures in parking garages, bridges, and marine applications. Chlorides have the ability to penetrate deeply into concrete, breakdown the protective film on the steel surface, and then initiate corrosion. The consequences of corrosion are cracking, delamination and spalling of the concrete cover, along with the loss of cross-sectional area and tensile capacity of the reinforcement. This may eventually lead to safety hazards and in extreme cases can cause loss of structural integrity and catastrophic failure. To this end, chloride prediction models (e.g., service life prediction models) are one of the primary tools used to estimate the time-to-corrosion initiation of reinforced concrete structures such as bridge decks.

In this research, the service lives of two bridges located in Durham Bridge on Route 8, New Brunswick, are investigated and evaluated. Ground-Penetrating Radar (GPR) is used to measure the actual cover thickness of the two bridges. Two service life prediction models that utilize the error function solution and Life-365 are used to evaluate the time-to-corrosion initiation of the two bridge decks, and two different concrete mix design mixtures (high performance concrete and normal concrete mixtures) are evaluated in the service life prediction models. The chloride transport properties of the high performance concrete are investigated in the laboratory. The influence of the most decisive parameters – time-dependent diffusion coefficient, time-dependent surface concentration and cover thickness – on the time-to-corrosion are likewise investigated and evaluated.

The GPR results showed a large variation in the cover thickness of the two bridge decks, with an average value of 50 mm and 60 mm being recorded for the Upper and Lower Durham bridges, respectively. The results of the chloride models reveal that the time-dependent diffusion coefficient, time-dependent surface concentration and cover thickness have a significant effect on the predicted service life of the two reinforced concrete bridge decks. However, of these three factors, cover thickness exhibits the greatest influence on the predicted time-to-corrosion initiation of the two bridge decks. In contrast, the results of predictive modelling based on the constant diffusion coefficient provide the lowest and most conservative service life prediction.

LIST OF ABBREVIATIONS AND SYMBOLS USED

ASTM	American Society for Testing and Materials
C	Total chloride concentration or content
C_f	Free chloride concentration or content
C_i	Initial free chloride concentration of host solution
C_s	Chloride surface concentration
CSH	Calcium Silicate Hydrates
CTH	Chalmers Tekniska Högskola (Common name for rapid migration test)
D	Chloride diffusion coefficient
D_a	Apparent chloride diffusion coefficient
D_{a28}	Instantaneous apparent diffusion coefficient at concrete age of 28 days
D_{AVG}	Average chloride diffusion coefficient
D_{nssm}	Non-steady state chloride migration coefficient
D_{ref}	Chloride diffusion coefficient at reference time and temperature
D(t)	Chloride diffusion coefficient at time t
E_a	Activation energy of cementitious system
erf	Error function
erfc	Complementary error function
F	Chloride flux
HPC	High performance concrete
i	Particular slice of concrete
L	Thickness of the specimen
m	Age parameter or age factor or reduction coefficient
m_{avg}	Age parameter as determined based on the average time method
m_e	Age parameter in the nonlinear model
m_{eff}	Age parameter as determined from the effective time method
m_{tot}	Age parameter as determined from the total time method
NC	Normal concrete
n	Time step
PC	Portland cement

pH	Concrete alkalinity
X	Variable distance from concrete surface
X_d	Average chloride penetration depth
S	Constant environmental factor
T	Time-dependent diffusion coefficient in error function solution
T	Temperature
T_{ref}	Reference temperature
t	Exposure time
t_{28}	Concrete age at 28 days
t_1	Concrete age at the start of exposure
t_2	Concrete age at the end of exposure
t_{avg}	Average time
t_{tot}	Total time (time at the end of exposure)
t_{eff}	Effective time
t_{ex}	Exposure time
t_{ref}	Reference time
U	Potential difference between both ends of the specimen
W/C	Water to cement ratio
Δt	Time step
Δx	Concrete slice thickness (total depth divided by number of slices)
u_i^n	Chloride concentration at time n and slice i
Ψ_p	Error function special function

1 INTRODUCTION

1.1 General

Chloride ingress into concrete continues to be a major cause of deterioration in reinforced concrete structures exposed to marine and deicing salt environments. Reinforced concrete structures such as wharves and piers, highway bridge decks, and parking garage structures frequently suffer from chloride attacks, which cause corrosion of the reinforcement. These structures are often designed to be durable and are expected to require minimum repair and maintenance during their lifetime. However, many marine structures and bridge decks show premature deterioration and require early repair and maintenance as a result of reinforcement corrosion deterioration caused by the penetration of chloride ions (Mehta 1991).

Corrosion of reinforced concrete structures exposed to a chloride environment is a common occurrence. Corrosive action on these structures can be highly detrimental and can lead to significant structural and economic loss. For instance, it has been reported that 50% of maintenance expenditures in Western Europe are spent on the repair and remediation of existing reinforced concrete structures deteriorated by corrosion of the reinforcement (Long et al. 2001). In the United States, approximately 23% of all bridges have deteriorated and require immediate repair, while about 39% are considered unreliable. The estimated repair cost of these structures is estimated to be in the range of USD $100 billion (Status of the Nations Highways and Bridges July 2, 1991). Therefore, a proper understanding of chloride penetration into concrete and the factors influencing the ingress of chloride ions are needed for proper estimation of a structure's service life.

Among several possible mechanisms, the diffusion process is considered the main one responsible for driving chloride ions into saturated concrete cover. Diffusion is defined as the movement of chloride ions under the action of a concentration gradient, where chloride ions move from regions of high chloride concentrations to those of low chloride concentrations through the concrete cover depth (Luping and Gulikers 2007). Other chloride mechanisms include convection, permeation, and migration. The convection process occurs in partially dry concrete cover, where chlorides move with moisture inside the concrete, and permeation takes place as a result of differences in hydraulic pressure in veracious zones. Migration occurs under the action of an electrical field potential (Poulsen, Ervin.,Mejlbro, Leif., 2006). In this thesis, the diffusion mechanism is considered the predominant mechanism of chloride transport into saturated concrete, and only chloride diffusion models are considered for service life prediction models.

There are mainly two types of chloride models reported in the published literature commonly used in modeling chloride ingress into concrete (Nilsson 2009). These models are the well-known error function solution with constant and time-dependent diffusion coefficients, and finite difference models such as Life-365. The error function solution is the simplest chloride model and is based on Fick's second law of diffusion. It is a popular chloride model often used by engineers in the field to estimate the service life of reinforced concrete structures. This model uses the total chloride measurement, also known as acid-soluble chloride profiles, which are usually determined experimentally to quantify the chloride diffusion coefficient and surface chloride concentration. These parameters are determined by fitting the error function solution equation to the measured chloride profiles using the least squared error method (Nilsson 2009). To determine the time-

dependent diffusion coefficient, multiple chloride profiles maintained at different exposure periods and concrete ages of the same concrete are required.

The other type of chloride model uses the finite difference approach. An example of this type of model is Life-365, which utilizes a concrete mix design to estimate the chloride diffusion coefficient and age parameter (m-value). It also takes into account the influence of time and temperature on the chloride diffusion coefficient as well as the time-dependent surface concentration. The main advantage of using the finite difference model over the simplified error function solution is that the projected diffusion coefficient is an instantaneous approach that takes into account the influence of time and temperature and thus results in a more accurate estimation of concrete service life. As a consequence, the finite difference model is more powerful and thus more frequently recommended for service life predictions for structures exposed to chloride environments.

1.2 Thesis Objectives

The objective of this thesis is to establish chloride transport parameters using the bulk diffusion test standard in order to estimate the service life of two bridges built in New Brunswick and to identify the influence of different concrete mix design proportions, exposure time, and cover thickness on the time-to-corrosion initiation of the reinforcement of the constructed bridge decks. Two chloride models are used for this purpose: the error function solution, with both constant and time-dependent diffusion coefficients, and Life-365. The Life-365 model allows for the evaluation of temperature and time-dependent surface concentration on the predicted service life of the two bridges.

1.3 Thesis Structure

This thesis consists of six chapters and appendices. The content and description of each chapter is given below:

Chapter 1: Introduction

Chapter 1 provides a general introduction to the research area and highlights the importance of modeling chloride ingress into concrete. It includes the major chloride transport processes, different chloride models, and some decisive parameters influencing chloride ingress into concrete as well as the objectives and the structure of this thesis.

Chapter 2: Literature Review

Chapter 2 provides a general background and overview of the causes of reinforced concrete deterioration and chloride diffusion. It specifically covers the corrosion of reinforcement as a major reason for structural deterioration; the causes of corrosion initiation in concrete, focusing on chloride attacks; the chloride diffusion theory and Fick's laws; the factors influencing chloride ingress into concrete; and common chloride test procedures.

Chapter 3: Prediction of Chloride Ingress Using Fick's Second Law of Diffusion

Chapter 3 provides an overview of the existing chloride models. The discussion in this chapter is directed to the error function solution, time-dependent diffusion coefficient, determination of the age parameter, the use of the finite difference approach, and a general description of Life-365.

Chapter 4: Experimental Program

In this chapter, a full description of the concrete mix design, sample preparations, and all test procedures used in this thesis are presented. The experimental data and test results are used to evaluate the service life prediction of the two Durham bridges investigated in this work.

Chapter 5: Results and Discussion

Chapter 5 covers the results and discussions of the field and laboratory data. The chloride parameters of the error function solution model for both water-soluble and acid-soluble chlorides are provided and discussed. The factors influencing the chloride penetration and service life predictions are highlighted and evaluated.

Chapter 6: Conclusions and Future Research

The final chapter covers the main conclusions drawn from the results and material presented in this thesis. Some suggestions for future investigations and research are also outlined.

2 LITERATURE REVIEW

This chapter provides a general literature review of the deterioration causes of reinforced concrete structures exposed to chloride environments. The main discussions of this chapter focus on reinforcement corrosion as the main cause of structural distress, chloride transport and Fick's laws, factors influencing chloride ingress into concrete, and some common chloride test procedures used to quantify chloride transport parameters, such as diffusion coefficients.

2.1 Reinforcement Corrosion of Concrete Structures

Reinforcement corrosion in reinforced concrete structures exposed to marine or deicing salts is a major concern and in many cases is considered the main cause of deterioration. This is because chloride ions have the ability to penetrate deeply into the concrete skin cover to the level of the reinforcement and initiate corrosion (Ahmad 2003). The high alkalinity of the concrete material is believed to provide a protection for reinforcing steel, which, in concrete, is often protected by a passive thin layer of iron oxide. This protective film is developed on the steel surface as a result of the high alkalinity (pH value) of the concrete pore solution, which is reported to be in the range of 13 to 14 (Ipavec et al. 2013). The protective film remains stable as long as the alkalinity of the concrete does not drop below a certain level or when no sufficient chloride ions accumulate in the vicinity of the reinforcement.

Previous research has shown that the depassivation of the protective film can occur only when either the concrete pH value drops to less than 9 or chloride ions accumulate in the vicinity of the reinforcement in a sufficient amount called the chloride threshold (Mehta 1991). Once the passive film is destroyed or broken down by carbonation or chlorides in the presence of oxygen and

moisture, corrosion is initiated. The initiation of corrosion causes volumetric changes in the concrete-steel interface, leading to tension stresses, the eventual consequence of which is the cracking and spalling of the concrete cover, as illustrated in Figure 2.1.

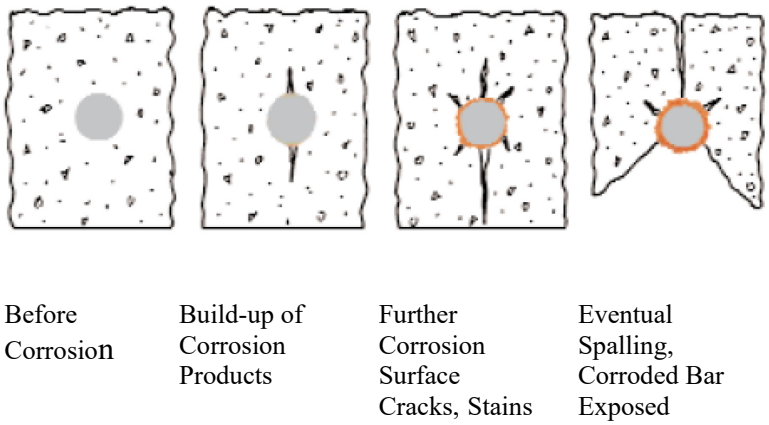

Figure 2.1 Influence of reinforcing steel on surrounding concrete

If no repair is made at this stage, the corrosion of reinforcing steel proceeds further, causing severe damage and deterioration to the structure and eventually leading to safety hazards and loss of structural integrity. The corrosion damage of a bridge structure is shown in Figure 2.2.

Due to the importance of corrosion in reinforced concrete structures, which is often considered the main cause of deterioration of marine structures, a brief description of the corrosion mechanism and its fundamentals is given in the following subsections.

Figure 2.2 Corrosion deterioration of bridge structure

2.2 Corrosion Mechanism and Its Fundamentals

According to (Bentur, A., Diamond, S., & Berke 1997) the corrosion of reinforcing steel is an electrochemical process that involves both chemical reactions and a flow of electrical current acting simultaneously. The chemical reactions take place at two different sites on the steel surface, as shown in Figure 2.3, and are known as an anodic reaction and a cathodic reaction, or simply anode and cathode.

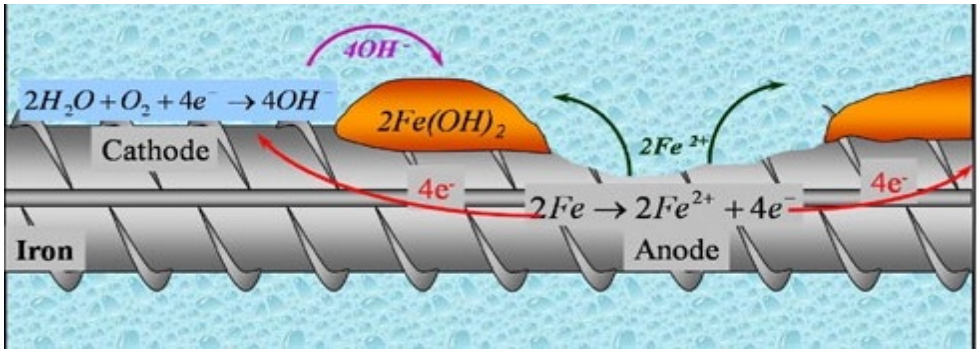

Figure 2.3 Electrochemical corrosion process on steel surface

Anodic reaction

$2Fe - 4e^- \longrightarrow 2Fe^{2+}$

Cathodic reaction

$O^{2-} + 2H2O + 4e^- \longrightarrow 4(OH^-)$

An electrical current must flow in a closed loop between the two sites in order for the two chemical reactions mentioned above to proceed. Two electrical currents flow in a closed loop occurring between the anode and cathode sites; the one within the steel is called the internal current, and the other one takes place through the pore solution surrounding the steel bars. The electrical current within the steel bar results from the flow of electrons from the anode to the cathode, which makes it an internal current. The movement of negatively charged ions in the surrounding pore solution establishes the external electrical current. The external current consists of hydroxide ions moving from the cathode to the anode, as indicated in Figure 2.3. The moving iron ions (Fe^{2+}) and hydroxide (OH^-) ions flow toward one another; when they meet, they react to form rust products ($Fe(OH)_2$), as indicated by the following reaction:

$2Fe^{2+} + 4OH^- \longrightarrow 2Fe(OH)_2$ (rust)

It should be noted that the corrosion of embedded steel in concrete would not occur as long as the protective layer of iron oxide remains stable. In other words, the two chemical reactions (e.g., anode and cathode) as well as the electrical current will not establish if the steel surface remains passive and protected by an impermeable concrete cover. However, both field and laboratory observations have shown that the protective film that develops on a steel surface can be impaired

if carbonation of the concrete cover or ingress of chloride ions to the depth of steel take place. Both carbonation and the penetration of chloride ions have the ability to destroy or depassivate the protective film and thus initiate the corrosion of reinforcement (Aït Mokhtar, K., Loche, J-M. Friedmann, H. Amiri, O. Ammar A. 2007). In the following subsections, the depassivation of steel surface by carbonation and chloride ions is briefly discussed.

2.3 Depassivation of Steel Protective Layer by Carbonation

Carbonation is a process in which carbon dioxide penetrates into the concrete surface and chemically reacts with the hydration products of the cement, such as calcium Silicate Hydroxide, CSH gel, alkali, and calcium ions. These reactions lead to a drastic reduction in the alkalinity of the concrete cover to levels of about pH 8. The time it takes for carbonation to reach the level of the reinforcement is a function of the properties of the concrete cover and the rate of the diffusion of the carbon dioxide. Corrosion of the reinforcement due to carbonation in modern concrete made with supplementary cementious materials is a relatively low probability and requires dry surfaces to proceed. Therefore, for modern concrete is concrete contains supplementary cementious materials such as fly ash, silica fume and slag that is fully saturated concrete, carbonation is seldom a matter of concern (Bentur, A., Diamond, S., & Berke 1997; Mehta 1991).

2.4 Depassivation of Steel Protective Layer by Ingress of Chloride Ions

A common cause for the depassivation of a steel surface is the penetration of chloride ions to the depth of that surface. Chloride ions have the ability to penetrate deeply into the concrete cover to the level of reinforcement and break down the passive layer that protects steel from corrosion, even at high alkalinity levels (Angst et al. 2009). For chloride ions to depassivate the steel surface and initiate corrosion, they need to reach a certain concentration at the level of the reinforcement,

called the chloride threshold. This threshold is a function of the net balance between the stability of the hydroxide ions and the disruption of the passive film by chloride ions. Husman (Hausman D.A., 1967) suggested that the chloride threshold concentration is about 0.61 times the hydroxide ion concentration for normal concrete mixtures made with ordinary Portland cement. That means that the chloride ion concentration Cl^- to hydroxide ion concentration OH^- ratio must be at least 0.61 or higher for chloride to initiate corrosion of the reinforcement.

In field practice, chloride concentration is often expressed as a percentage of total chloride content. This percentage is usually specified by weight or volume of the cement or binder used. Sometimes, the chloride threshold is specified in terms of the weight of chlorides per unit volume of concrete, in the range of 0.9 to 1.2 kg/m^3. This corresponds to 0.05% to 1% by weight of concrete or 0.3% to 0.4% by weight of cement (Angst et al. 2009). Many concrete codes and specifications put limits on the background chloride content in concrete and background chloride means chloride exist in concrete before exposure (e.g., in mixing water aggregates, etc.). For instance, the American Concrete Institute (ACI) limits the amount of chloride content for conventional reinforced concrete to 0.1%.

2.5 Factors Influencing Corrosion of Reinforcing Steel in Concrete

From the consideration of the corrosion mechanism and the deterioration process of concrete as a result of corrosion, it appears that the time required to depassivate steel surfaces in reinforced concrete is a function of several factors, including cement type and composition, the chloride content of concrete, the availability of oxygen and moisture in the vicinity of the reinforcement, and the concrete cover thickness provided. Some of these factors are discussed in the following subsections.

2.5.1 Cement Type, Compositions and W/C Ratio

Many researchers and workers have suggested that cement type, composition, and inclusion of Supplementary Cementitious Materials (SCMs) play an important role in controlling the rate at which aggressive ions such as chlorides penetrate into concrete (Jones et al. 1997; Byfors 1987; Page et al. 1981; Thomas et al. 2012). Additionally, laboratory and field observations and data have shown that difference in cement or binder types can play a significant role in limiting chloride-induced corrosion. It was suggested that cement with high alumina content (C_3A) would perform far better in reducing chloride ingress due to its ability to chemically bind chlorides in the form of Friedl's salt and prevent them from reaching the reinforcement (Byfors 1986). The physical properties of the cement, such as its fineness and surface area, are considered important factors in refining the pore structure and increasing the tortuosity, and thus reducing the rate at which chloride ions diffuse in concrete (Song et al. 2012; Chalee and Jaturapitakkul 2009). Due to their physical properties and chemical compositions, the addition of SCMs such as fly ash, silica fume and blast furnace slag cement have been found to greatly improve concrete and protect the reinforcement from chloride attacks (Thomas et al. 1999; Pavlik et al. 2010). The addition of SCMs enhances the concrete resistance to chloride penetration by reducing the porosity and improving the impermeability of concrete microstructure Therefore, the use of a high quality concrete mixture that incorporates reasonable levels of SCMs (with a low w/c ratio) has become good practice for reinforced concrete structures built in severe environmental conditions, such as chloride environments.

The diffusion of chloride ions into concrete is sensitive to the degree of hydration, density and interconnectivity of the concrete pore structure system, which is mainly controlled by the w/c ratio

of the concrete mixture (Murthi and Sivakumar 2008). When concrete is made with a low w/c ratio, the pore structure is primarily tortuous and discontinuous, so the chloride diffusion rate will be very small. However, for concrete made with a high w/c ratio, the pore system will be more porous, extensively interconnected and continuous, due to the formation of larger pores. This will facilitate the ingress of chloride ions, which will result in faster ion transport and a larger rate of chloride diffusion (Mehta and Monteiro 2006).

It must be remembered that good construction practices (i.e., proper placement, consolidation and curing, adequate depth of concrete cover, etc.) are still required in order to maintain the intended concrete durability even when high quality concrete mix design is provided.

2.5.2 Availability of Oxygen and Moisture in the Vicinity of Reinforcement

The corrosion of reinforcing steel will not initiate if there is not enough dissolved oxygen and moisture in the vicinity of the reinforcement, even when the passive film is partially or completely destroyed by chloride ions. This is because the availability of oxygen and moisture at the steel surface is a condition for the chemical reactions to occur. Mehta (1991) reported that for the oxygen to take part in the chemical reactions at the cathode, it must be in a dissolved state, as both permeability and cover thickness affect the availability of oxygen at the reinforcement level.

2.5.3 Inadequate Concrete Cover Thickness

The time required for corrosion of the reinforcing steel to initiate and the rate at which chloride ions diffuse through the concrete will strongly depend on the thickness and nature of the concrete cover depth provided. Many concrete codes and specifications require a minimum of 50 mm or higher concrete cover thickness for reinforced concrete structures exposed to severe environmental

conditions, such as marine and deicing salt environments (Angst et al. 2009). The cover thickness is considered the first line of defense for reinforcement against chloride attacks. Thus, cover thickness is a key parameter in the durability design and redesign of reinforced concrete structures exposed to aggressive environments.

In practice, providing a consistent cover thickness over the reinforcement is not an easy task and in many cases not even applicable. Depth variations in concrete cover thickness during construction are a common problem in structures such as bridge decks, parking garages, and marine structures. An inadequate concrete cover can significantly reduce the time-to-corrosion initiation, which will result in short lifetime expectancy. A recent study conducted by Omer (Omer 2016) showed that cover thickness can greatly influence the service life of reinforced concrete structures with respect to corrosion. He further stated that a good correlation is found between the predicted service life and the concrete cover thickness over the reinforcement, as indicated in Figure 2.4. Boddy et al. (Boddy et al. 1999) reported similar observations. Field studies and inspections suggest that the premature deterioration of many reinforced concrete structures is primarily related to the application of inadequate concrete cover thickness, which shortens the time required for corrosion to initiate.

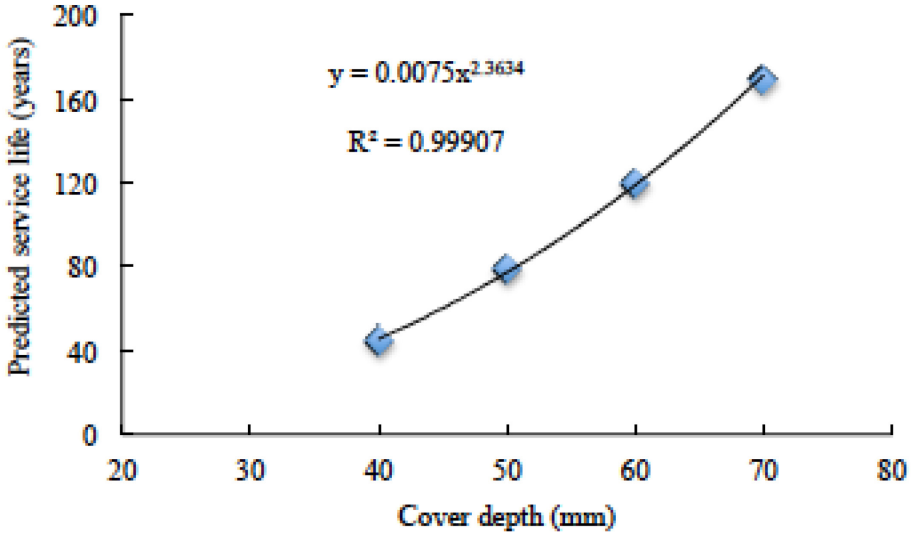

Figure 2.4 Influence of cover thickness on the predicted service life (Omer 2016)

2.6 Chloride Transport

Depending on the moisture or saturation levels of concrete, different chloride transport mechanisms may result. In fully saturated concrete, the diffusion process is considered the predominant transport process for chloride ions in a concrete pore solution. Diffusion is defined as the movement of chloride ions under the action of a concentration gradient, where chloride ions move from regions of high chloride concentrations of concrete cover depth to those of low chloride concentrations (Luping 1996). In dry or partially dry concrete, absorption or convection may interact with diffusion to move chloride ions inside a concrete cover. Convection is a chloride transport process in which the chlorides move with moisture inside the concrete. It is essentially a rapid transport process that is limited to the depth of the dry portion of the cover skin. Other transport processes include permeation and migration. Permeation takes place when one side of a concrete structure is subjected to hydraulic pressure, as in the case of an underwater quay wall or returned walls. Migration occurs under the action of an electrical field potential (Poulsen,

Ervin.,Mejlbro, Leif., 2006). In this thesis, the concrete is assumed to be fully saturated, so the diffusion mechanism is considered as the predominant mechanism of chloride transport in concrete. Fick's laws are highly relevant in modeling chloride ingress into concrete and are thus widely used in chloride transport and service life models.

2.6.1 Diffusion Theory Based on Fick's Laws

Chloride penetration into saturated concrete is often modeled by means of Fick's first and second laws of diffusion. According to Poulson and Mejlbro (Poulsen, Ervin.,Mejlbro, Leif., 2006), the theory of diffusion was first introduced by Eugen Fick in 1829, who proposed a mathematical expression for the diffusion of heat movement. Later, the two well-known mathematical expressions of the diffusion theory known as Fick's first and second laws were widely applied to model chloride transport in concrete. Nilsson (Nilsson 2009) reported that Collepardie et al. (1970, 1972) were the first to apply Fick's laws to model chloride ingress into concrete. Fick's first and second laws as used in modeling chloride ingress into concrete are presented below.

2.6.1.1 Fick's First Law

Under the assumption of the steady state of diffusion, where the chloride concentration does not change with time, the flux, F, is proportional to the concentration gradient. The diffusion flux moves from a region of high concentration to one of low concentration. This has been expressed as shown in Equation (2.1):

$$F = - D_{eff} \cdot \frac{\partial C_f}{\partial x} \quad \text{..... (2.1)}$$

where:

F: the diffusion flux of free chloride ions per unit area of concrete per unit time ($kg/m^2.s$)

D_{eff}: the effective diffusion coefficient or diffusivity (m^2/s)

C_f: the chloride free concentration, (kg/m^3 of solution)

X: a variable distance from the surface, the dimension of which is length (m)

Fick's first law describes the movement of free chloride ions in the pore solution when there is no change in the chloride concentration. This means that the effective diffusion coefficient is constant and does not change either with concentration or time. Therefore, Fick's first law is valid only when the steady state is established (i.e., when the concentration becomes constant with time). However, in concrete material, the flux of chloride ions is not constant and the concentration at any point in time changes as chloride ions diffuse. This has led to the derivation of Fick's second law, which can describe the chloride when the non-steady state is the case.

2.6.1.2 Fick's Second Law

As mentioned above, Fick's first law is only useful for a steady-state condition where the chloride concentration is constant over time. However, in concrete, chloride concentrations change with time as well as with position. This condition is called the non-steady state of chloride diffusion. Therefore, Fick's first law may not be valid for describing the movement of chloride ions in concrete under the condition of non-steady state. However, it has been used as a baseline to derive the relevant Fick's second law of diffusion, which describes the movement or transport of chloride ions in a concrete medium under the non-steady state condition, as shown in Equations (2.2) to (2.5):

$$\frac{\partial C}{\partial t} = -\frac{\partial F}{\partial x} \quad \text{..... (2.3)}$$

$$\frac{\partial C}{\partial t} = \frac{\partial}{\partial x}\left(D_{eff}\frac{\partial C_f}{\partial x}\right) \quad \text{(2.4)}$$

$$\frac{\partial C}{\partial t} = D\frac{\partial^2 C}{\partial x^2} \quad \text{(2.5)}$$

Fick's second law, as shown in Equation (2.5), simply states that the change in chloride concentration per unit time is equal to the change of flux, F, per unit length. This law is sometimes referred to as the mass balance equation of chloride transport in concrete (Poulsen, Ervin.,Mejlbro, Leif., 2006). Equation (2.5) is often used to describe the movement of total chloride content, C, in concrete. In this case, the diffusion coefficient is referred to as the apparent diffusion coefficient, D_a (m^2/s), (Omer 2016).

Equation (2.5) is the well-known Fick's second law and has been widely used in chloride prediction models to describe the movement of chloride ions in concrete. Two typical solutions have been commonly used to solve Eq. (2.5). These two solutions are the well-known error function solution and the finite difference approach. These solutions and their assumptions are discussed in detail in Chapter 3.

2.6.2 Factors Influencing Chloride Transport in Concrete

Chloride transport in concrete is influenced by many factors, including chloride binding, concrete mix design and proportions, and environmental exposure conditions. A brief description of each of these factors is provided below.

2.6.2.1 Chloride Binding

Chloride binding is defined as the ability of concrete to bind chloride ions and thus remove them from the pore solution. Numerous researchers and studies have confirmed that when chloride ions are either internally or externally introduced to concrete, some are captured by the hydration products of the cement (Arya et al. 1990; Neville 1996; Zibara 2001; Luping and Nilsson 1993). Two types of binding occur in concrete: physical binding and chemical binding. Physical binding takes place when chloride ions physically adsorb or adhere to the calcium silicate hydrates gel (C-S-H) surfaces, while chemical binding occurs when the introduced chloride ions chemically react with the aluminate content of the cement to form what is known as Friedel's salt.

According to Martin-Perez et al. (Martin-Perez et al. 2000), binding can influence the diffusion of chloride ions as follows: First, it slows down the movement of chloride ions in the pore solution; secondly, it reduces the chloride concentration at the depth of the reinforcement and thus increases the time to corrosion initiation; and finally, when Friedel's salt is formed (which alters the pore structure and reduces the concrete porosity), it increases the resistance of concrete to the ingress of new chlorides (Omer 2016). Binding also has a direct influence on the chloride concentration on the concrete surface, Cs. Specifically, the surface concentration will be high if the binding capacity of the concrete is high. This implies that for different exposure conditions, different concrete mixtures can have different binding capacities and surface chloride concentrations.

2.6.2.2 Influence of Concrete Mix Design and Cement Type

The concrete mix design – mainly the w/c ratio and type of cement or binder used – plays a significant role in controlling chloride ingress and the overall durability of the concrete. Previous studies and field data show that concrete made with a low w/c ratio and incorporating a high

volume of supplementary cementitious materials can significantly reduce the chloride transport and limit its diffusion rate (Page et al. 1981; Song et al. 2011; Song et al. 2012; Thomas and Bamforth 1999). A low w/c ratio results in a dense concrete with low permeability and high resistance to chloride penetration.

Page et al. (Page et al. 1981) studied the chloride diffusion of concrete mixtures made with different w/c ratios and found that the chloride diffusion of concrete made with a 0.6 w/c ratio was 6 times higher than that made with a 0.4 w/c ratio. The incorporation of SCMs was also found to sharply reduce the rate at which chloride transports into concrete. The addition of silica fume, fly ash and slag cement at different rates of replacements were found to greatly refine the pore structure, increase the tortuosity of the pore system, and lower the concrete porosity to a great extent (Bjegovic et al. 2012; Burris and Riding 2014; Bouikni et al. 2009). The influence of fly ash and slag cement is also related to their high alumina content, which is responsible for the chemical binding that takes place within the concrete microstructure system. Silica fume contributes to the reduction in the chloride transport rates at early ages due to its high surface area and ultra-fine particles. These can physically reduce the interconnectivity of the pore system by subdividing larger pores in discontinuous and smaller pores, which can then significantly narrow the pore channels and their networks (Thomas et al. 2012).

2.6.2.3 Environmental Exposure Conditions

The penetration of chlorides into concrete and its rate of diffusion have been found to be a function of the type of environmental exposure conditions. For instance, the concentration of chloride ions in a marine environment is different from that in a deicing salt environment. Specifically, the chloride concentration in a marine environment is relatively smaller and less aggressive. Another

important environmental factor that was found to strongly influence the rate of chloride diffusion into concrete is ambient temperature. The chloride diffusion rate was found to increase with temperature, and vice-versa (Omer et al. 2015). This is because temperature changes the chloride transport by modifying the transport rate of chloride ions and altering the hydration rate of cement paste (Riding et al. 2013). Higher temperatures accelerate the rate of chloride diffusion, leading to faster penetration of chloride ions into concrete, whereas lower temperatures decrease the rate of chloride diffusion and thus slow down the penetration rate. Several researchers suggested that the influence of temperature on chloride ionic diffusivity obeys the Arrhenius relationship of temperature (Luping 1996; Boddy et al. 1999). The Arrhenius relationship is often used in chloride models to account for the influence of temperature on chloride diffusivity (Omer 2016).

2.7 Chloride Test Methods

Several test methods for chloride penetration in concrete have been proposed and standardized over the past decades (Stanish, K.D., Hooton, R.D., and Thomas, M.D.A. 1997). Almost all existing chloride test methods used to determine chloride diffusivity involve the determination of chloride content in concrete test specimens. In North America, the common test method for chloride diffusivity is the bulk diffusion test, as standardized by ASTM C1556, which involves the determination of the apparent chloride diffusion coefficient and surface concentration of the concrete. In Europe, the Nordic test methods are commonly used to measure chloride diffusion or migration into concrete. Examples of these methods include: NordTest NT build 443 and NordTest NT build 492. Other test methods used to indicate the ability of concrete to resist chloride penetration include: the Rapid Chloride Pearmeability Test (RCPT – ASTM C1202), and resistivity and pressure penetration techniques (Shi et al. 2012). While not quantitative, these test methods still provide a good indication of concrete resistance to the penetration of chloride ions

and are often used for comparison purposes of different concrete mixtures. In the following sections, the two most common quantitative chloride test methods used to determine chloride diffusion coefficients are presented.

2.7.1 Bulk Diffusion Test Method ASTM C1556

This test method covers the determination of the apparent chloride diffusion coefficient of hardened concrete samples. In this test, a saturated concrete specimen is immersed in a high chloride concentration solution for a specified period of time. The high concentration is chosen to shorten the test duration. The test specimen is sealed on all surfaces except one, across which the diffusion can occur; it is also saturated with limewater prior to exposure to the chloride solution to avoid any capillary effects of the specimen-exposed surface. Next, the specimen is exposed to chloride by immersion in a solution containing 165 g of sodium chloride (NaCl) per liter at a temperature of 23 ± 1° C for a minimum period of 35 days. At the end of the exposure period, the chloride penetration profile is determined by collecting concrete powder samples at different depths from the exposed surface in steps of 1 mm. A chemical analysis, usually acid-soluble chloride, is conducted to determine the total chloride content in each powder sample. The chloride concentrations are then plotted at their corresponding depths, as shown in Figure 2.5. Once the chloride profile is established, chloride parameters, including chloride initial concentration (C_i), surface concentration (C_s) and apparent chloride diffusion coefficient (D_a), are determined by fitting the error function solution, shown in Equation (2.6), to the measured chloride profile using a non-linear regression analysis following the least squared method.

$$C(x,t) = C_s - (C_s - C_i) \cdot \operatorname{erf}\left(\frac{x}{\sqrt{4 \cdot D_a \cdot t}}\right) \quad \text{..... (2.6)}$$

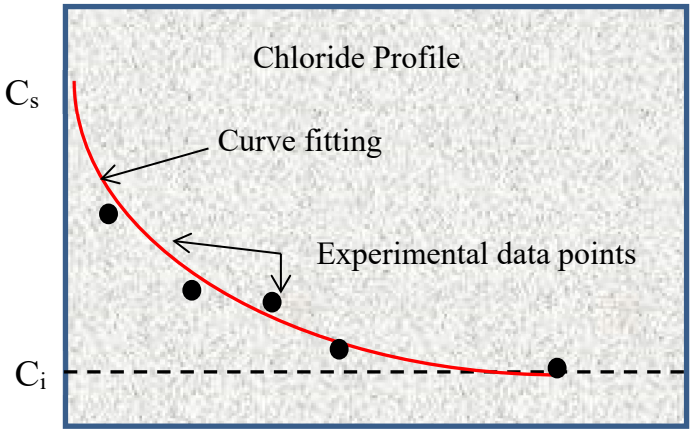

Figure 2.5 Nonlinear regression analysis of measured chloride concentration profile

The calculated diffusion coefficient, D_a, is often directly used to calculate the future chloride concentration at different depths for concrete exposed to chloride environments. However, this may not be accurate without taking into account the effect of other factors, as will be discussed in Chapter 3.

2.7.2 Rapid Migration Test Method NordTest NT BUILD 492

Luping and Nilsson (Luping and Nilsson 1992) developed a rapid migration test method, also known as the CTH test. This abbreviation refers to the name of the university in which the test method was developed (Chalmers Tekniska Hogskola). The rapid migration test is a non-steady state migration test that uses an electrical potential to force chloride ions to penetrate through a concrete specimen. A 50 mm-thick test specimen is placed between two solutions, with the upper surface exposed to 0.3 M sodium hydroxide and the bottom surface exposed to 10% sodium chloride solution, as shown in Figure 2.6. A voltage of 30 V is applied through the specimen for a period of 24 hours.

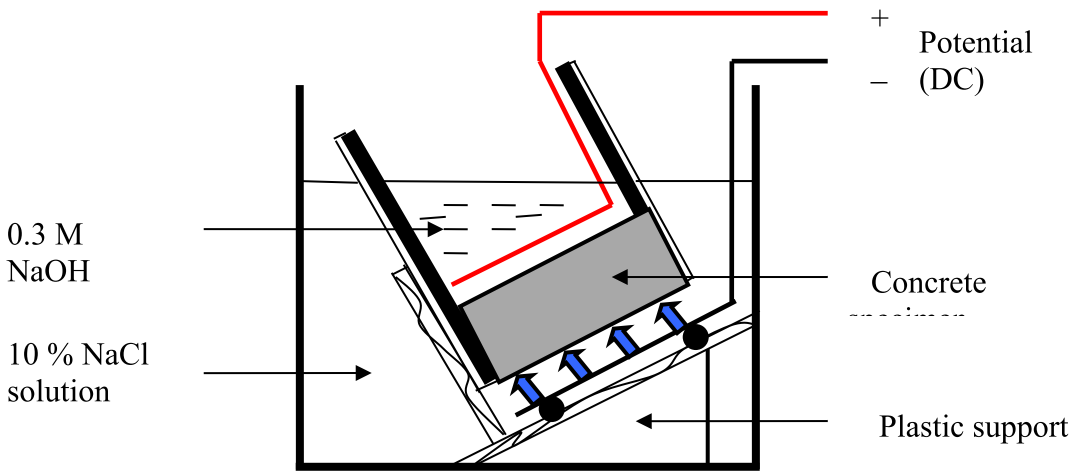

Figure 2.6 Chloride migration test set-up

At the end of the test, the concrete specimen is removed and axially split into two halves. A nitric silver solution is sprayed on one of the fresh surfaces to detect the depth of the chloride penetration. Usually seven depth readings are measured at intervals of 10 mm, and the average depth is then used in Equation (2.7) to calculate the chloride migration coefficient.

$$D_{nssm} = \frac{0.0239(173 + T)L}{(U - 2)t}\left(X_d 0.0238\sqrt{\frac{(173 + T)LX_d}{U - 2}}\right) \text{..................................} \quad (2.7)$$

where:

D_{nssm}: the migration coefficient, m^2/s,

U: the applied potential, V,

T: the average value of the initial and final temperature in 0.3 N NaOH solution, in ºC,

L: the thickness of the specimen, in mm, and

X_d: the average value of the penetration depths, in mm; and t is the test duration, in hours.

The main advantage of the rapid migration test over the bulk diffusion test is that it requires only 24 hours to complete and obtain a concrete diffusivity value, whereas the bulk diffusion test requires a minimum of 35 days (and sometimes up to 90 days) to get the results. The relatively long exposure period of the bulk diffusion test has also been found to affect the projected value of the apparent diffusion coefficient (Luping and Nilsson 1992). According to several researchers, the diffusion coefficient, as calculated using the bulk diffusion test, is the average of the changing diffusion coefficient over the testing period (Stanish and Thomas 2003). Therefore, the value of the diffusion coefficient changes reflects the exposure time during the test changes. Stanish and Thomas (2003) called the value of the diffusion coefficient as projected from the bulk diffusion test an average diffusion coefficient, D_{AVG}, that occurs at some point in time during the test period. The changes in the diffusivity value result from the changes that occur within the concrete matrix as a result of the ongoing hydration process, leading to a reduction in the porosity and pore volume over time. Therefore, the assumption that the diffusion coefficient remains constant during the testing is not valid.

In this thesis, the bulk diffusion test method is used to project chloride profiles, which are then used to determine chloride transport parameters of tested concrete specimens.

3 PREDICTION OF CHLORIDE INGRESS USING FICK'S SECOND LAW OF DIFFUSION

Fick's second law chloride models are widely used by researchers and engineers in the field for predicting and estimating the time-to-corrosion initiation caused by the penetration of chloride ions. Chloride models based on Fick's second law assume that chloride ions are inert ions and do not interact with other ions existing in the pore solution. It should be realized that Fick's second law chloride models aim to describe the physical and chemical outcomes of the movement of chloride ions in concrete. They do not, however, describe the actual physical and chemical interactions that take place within the concrete as result of chloride penetration (Fredriksen et al. 2008). Among other models, error function solution and Life-365 chloride models are the most common that use Fick's second law of diffusion to describe chloride ingress into concrete and predict the time-to-corrosion initiation of the reinforcement.

In this chapter, a description of the error function solution and its historical development in modeling chloride ingress into concrete is provided, followed by a description of a finite difference method and Life-365 model.

3.1 Error Function Solution Models

These models are widely used in modeling chloride ingress into concrete and predicting the time-to-corrosion initiation due to their simplicity and user-friendly features. In this section, the historical development of the error function solution is provided.

3.1.1 Collepardi's Model

According to Nilsson (Nilsson 2009), Collepardi et al. (1970, 1972) were the first to use Fick's second law of diffusion in modeling chloride ingress into saturated concrete. By applying the assumptions of homogeneous concrete, constant surface chloride concentration, constant diffusion coefficient, linear binding or constant binding capacity, and one-dimensional diffusion in a semi-infinite medium, Collepardi et al. used the error function solution to Fick's second law, as shown in Equation (3.1):

$$\frac{C}{C_s} = 1\text{-}\mathrm{erf}\left(\frac{x}{2\sqrt{D_a.t}}\right) \quad \text{..... (3.1)}$$

where:

C: the chloride concentration (% by weight of concrete)

C_s: the surface chloride concentration (% by weight of concrete),

erf: the error function,

D_a: the apparent diffusion coefficient (m^2/s), and

t: the time (sec).

By fitting the error function solution to the measured total chloride profiles (also known as acid-soluble profiles) using nonlinear regression, the surface chloride concentration, C_s, and the apparent diffusion coefficient, D_a, are determined as regression coefficients that give the best fit between the model and the experimental data. Once these parameters are determined, Equation (3.1) is then used to estimate the time-to-corrosion initiation at any depth from the exposed surface. In Collepardi's model, both the chloride diffusion coefficient and the surface chloride concentration are assumed constant during the exposure throughout the service life of the structure.

3.1.2 Time-dependent Diffusion Coefficient

The error function solution as presented in Equation (3.1) has been proven to be very conservative due to ignorance of the retarding influence on the diffusion process as a result of chloride binding and refinement of pore structure, which takes place as time elapses (Luping and Gulikers 2007). It was realized that the chloride ingress into concrete did not proceed as predicted by Equation (3.1), as per Collepardi's model. Takewaka and Matsumoto (Takewaka, K. and Mastumoto, S. 1988) were the first to note that the apparent diffusion coefficient is not constant but decreases with time due to binding and ongoing hydration of concrete. This was further confirmed by other researchers, including Maage et al. (1996), Poulson (1993), and (Maage et al. 1996; Poulsen 1993; Thomas and Bamforth 1999). Later, the influence of time on the diffusion coefficient was taken into account and the time-dependent diffusion concept was introduced. A commonly used expression for a time-dependent diffusion coefficient is shown in Equation (3.2), (Thomas and Bamforth 1999):

$$D(t) = D_{ref}\left(\frac{t_{ref}}{t}\right)^{m} \quad \text{..... (3.2)}$$

where

D(t): the diffusion coefficient at time t (m^2/s),

t: the time (sec),

D_{ref}: the diffusion coefficient at reference time t_{ref} (usually taken as 28 days), and

m: the age parameter or age factor stands for the reduction in the diffusion coefficient over time, also known as the m-value or decay parameter.

The D_{ref} and the value of m are often quantified experimentally using multiple chloride profiles obtained for the same concrete at different exposure periods or different ages. It should be noted that different values of m may result if different representative concrete ages are used. As reported by Nokken (Nokken et al. 2006), three techniques have been used in the literature to determine the value of m: the total time, t_{tot} (equal to the age of the sample at the end of exposure), the average time, t_{avg} (equal to the age of the sample before exposure plus the age of the sample at the end of exposure, divided by 2), and the effective time, t_{eff}, as given by Equation (3.3) and as proposed by Stanish and Thomas (Stanish and Thomas 2003):

$$t_{eff} = \begin{cases} \left[\dfrac{(1-m)(t_2-t_1)}{t_2^{\,1-m}-t_1^{\,1-m}}\right]^{1/m} & m \neq 0.1 \\ \dfrac{t_2-t_1}{\ln\left(\dfrac{t_2}{t_1}\right)} & m = 1 \end{cases} \qquad \text{(3.3)}$$

Previous work and studies have shown that the value of m is mostly dependent on the amount and type of cementitious materials involved in the concrete mix design. Extensive research done earlier by Bamforth (Bamforth 1996) showed that the value of m for concrete made only with Portland cement is about 0.25 and for that containing 30% Fly ash is about 0.62. The highest value of m was recorded for concrete containing 50% slag, which was about 0.7. According to Thomas and Bamforth (Thomas and Bamforth 1999), low values of m in the range of 0.2 to 0.3 can be used for normal concrete containing only ordinary Portland cement, while higher values in the range of 0.5 to 0.7 can be used for concrete incorporating 50% to 70% slag or 25% to 30% fly ash as a partial replacement of Portland cement. Other researchers have reported that the value of m is also influenced by the w/c ratio (L. Tang, H. E. Sørensen 2001; Poulsen, Ervin.,Mejlbro, Leif., 2006).

It has been reported that the lower the w/c ratio is, the higher the value of m will be. It should also be noted that the estimated service life of concrete structures is very sensitive to the value of m used. As concluded by Nokken, the service life is highly influenced by the value of m, and if this parameter is not properly determined, a significant bias in the predicted service life of the structure can be expected.

3.1.3 Mangat and Molloy Chloride Model

Mangat and Molloy (1994) developed the second version of the error function solution by including the time-dependent diffusion coefficient in the model. They replaced the constant diffusion coefficient, D_a, in Equation (3.1) by D(t) in Equation (3.2). To include the time-dependent diffusion coefficient equation in the error function solution, an integration of the diffusion coefficient with respect to time needs to be carried out. The proposed time-dependent error function solution as proposed by Mangat and Molloy is given by Equation (3.4):

$$C(x,t) = C_s \left[1\text{-erf}\left(\frac{x}{2\sqrt{T}}\right)\right] \quad \text{..... (3.4)}$$

where:

$$T = \int_0^t D(t)dt = \frac{D_{ref}}{1\text{-}m}\, t^{1-m} \quad \text{..... (3.5)}$$

More recently, Luping and Gulikers (2007) reported that a mathematical error in the time integration was mistakenly used by Mangat and Molloy in Equation (3.5). They corrected the expression in Equation (3.5), as shown in Equation (3.6):

$$T = \int_{t_1}^{t_1+t_{ex}} D(t)dt = \frac{D_{ref}(t_{ref})^m}{1-m}.\left[(t_{ex}+t_1)^{1-m}-(t_1)^{1-m}\right] \quad \text{..... (3.6)}$$

where t_1 is the age of concrete at the exposure and t_{ex} is the exposure period.

By including the time-dependent diffusion coefficient in the error function solution, more accurate service life is predicted compared to the error function solution with constant diffusion coefficient given in Equation (3.1), which results in a more conservative prediction of service life.

3.1.4 Time-dependent Surface Concentration

The third development of the error function solution came after it was discovered that the surface chloride concentration was also time-dependent. In the previous version of the error function solution, the surface concentration is taken as a constant during the exposure time. However, numerous studies have shown that the surface chloride concentration of the exposed concrete skin is not constant (at least not during the first a few years of exposure) but varies with the length of the exposure time and the chloride intensity of the environment (Mangat, P. S. and Molloy, B. T. 1994; Nilsson et al. 1996; Amey et al. 1998; Poulsen, Ervin.,Mejlbro, Leif., 2006; Ann et al. 2009; Song et al. 2009).

Field observations have shown that the build-up time of the surface concentration is limited to the first few years of exposure, beyond which the concentration becomes constant for the rest of the structure service life. The amount of surface chloride content and the time it takes to build up is a function of several factors, including the type of exposure environment (marine or deicing salts), concrete mixture proportions, the binding properties of the exposed concrete skin, and the washout effect on roadway structures. For marine environments, the built-up surface concentration varies with the type and conditions of the exposure zone. According to Poulsen and Mejlbro (2006), the

surface chloride concentration of the exposed concrete in marine splash and submerged zones may be taken as a constant after approximately 2 to 5 years, though it might take little longer for the atmosphere zone.

Practical experiences have also shown that the chloride concentration in the surface layer is anomalously decreased due to the fact that the concrete skin layer usually has a different microstructure than that of the internal concrete, as shown in Figure 3.1. The change in the microstructure of the concrete skin layer could be attributed to the finishing technique, wall effect, segregation, compaction, or washout effect (Andrade et al. 1997). This phenomenon is more noticeable in concrete structures exposed to an atmosphere zone. For this reason, some test standards recommend that the skin layer be cut or the chloride content of the exposed layer be disregarded when chloride profiles are obtained.

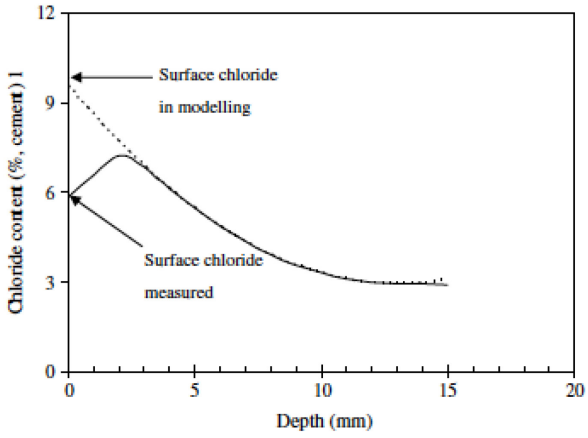

Figure 3.1 Reduction in the surface concentration of the measured chloride profile (Ann et al. 2009)

Determining the surface concentration build-up is not a straightforward process, as it requires observing the concrete response in under-determined environments and exposure conditions.

Several researchers have attempted to develop C_s models that can be readily incorporated in the error function solution to account for the change in the surface concentration with time (Mejlbro 1996; Poulsen, Ervin.,Mejlbro, Leif., 2006; Ann et al. 2009; Song et al. 2009; Chen et al. 2013).

3.1.5 Mejlbro's Model (HETEK Model)

Mejlbro (Mejlbro 1996) proposed a solution to Fick's second law to model chloride ingress into concrete, where both a time-dependent diffusion coefficient and time-dependent surface concentration are included in the model. He replaced the "erf" term with a special function, Ψ, to account for the time-dependent surface concentration as well as time-dependent diffusion coefficient. This model was later named the HETEK model, also known as the complete solution for Fick's second law. Mejlbro's model is shown in Equation (3.7)

$$C(x,t)=C_i+S\left(\int_{t_{ex}}^{t} D(\tau)d\tau\right)^{p}\Psi_p\left(\frac{x}{2\sqrt{\int_{t_{ex}}^{t} D(\tau)d\tau}}\right),\quad x\geq 0,\ t>t_{ex} \qquad (3.7)$$

Where S is a constant environmental factor.

Equation (3.7) is the up-to-date and most general error function solution to Fick's second law of diffusion of chloride ions in concrete. It is interesting to note that the simplified version of the error function solution with constant C_s and D_a is still widely used among engineers in the field, despite the existence of other versions providing more accurate estimations thanks to the inclusion of critical contributing factors.

3.2 Numerical Solution (Finite Difference Method) to Fick's Second Law of Diffusion

The Fick's 2nd law shown in Equation (2.5) is a partial deferential equation. Finite difference methods are very relevant to approximate partial differential equations, Ames (1977) and Newman (1991). Indeed, by using Taylor's series, it is possible to show that

$$\frac{u(x+h, y)- u(x, y)}{h} \quad \text{(3.8)}$$

or

$$\frac{u(x, y)-u(x-h, y)}{h} \quad \text{(3.9)}$$

are approximate expressions for h close to 0, of:

$$\frac{\partial u(x,y)}{\partial x}$$

Similarly:

$$\frac{u(x+h,\ y)-2u(x,y)+u(x-h,y)}{h^2} \quad \text{Eq. (3.10)}$$

is approximation of:

$$\frac{\partial^2 u(x,y)}{\partial x^2}$$

From these relations, any partial differential equation of the second order or less can be approximated. By defining grids in space and time, as shown in Figure 3.2, the approximation of u(x, t) is known for each node of the network. The partial differential equations are replaced by finite difference schemes, which have to be solved for each node x_i of the space grid and for each time step, Δt. The smaller the values of Δx and Δt, the higher the accuracy of the solutions obtained.

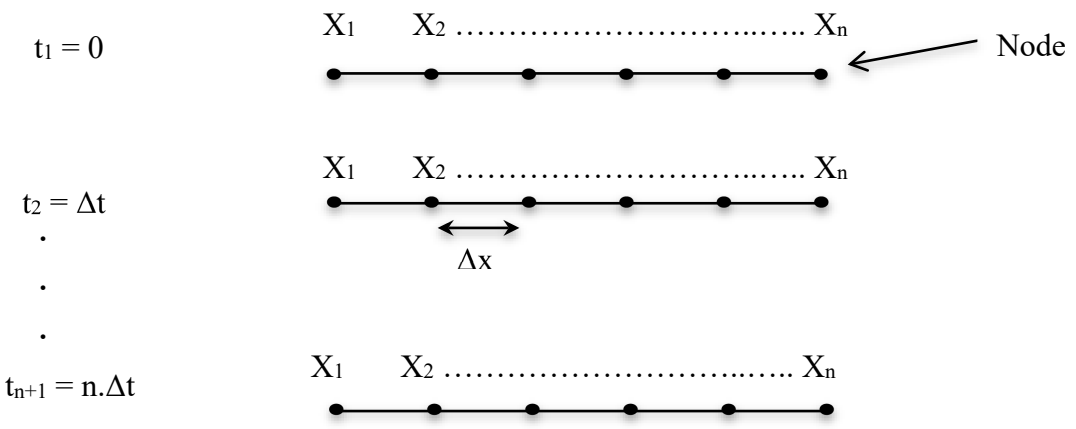

Figure 3.2 Finite difference grid approximations

where:

Δx: is increment depth (m) and Δt: is time increment (s).

Two common finite difference methods are typically used to solve the partial differential equations, such that Fick's 2nd law includes the Forward Euler and Crank-Nicholson methods.

The finite difference Forward scheme is shown in Equation (3.11):

$$\boldsymbol{u_i^{n+1} = u_i^n + \frac{D_c \Delta t}{\Delta x^2}(u_{i+1}^n - 2u_i^n + u_{i-1}^n)} \quad \text{……..…… (3.11)}$$

The Forward Euler method is an explicit model where the future concentrations are estimated based on the current chloride concentrations.

The Crank-Nicholson approach is an implicit technique involving the consideration of both current and future chloride concentration values in its solution. The level of chloride at a given slice of the concrete, I, and the next time period, t+1, is determined as shown in Equation (3.12)

$$-\boldsymbol{ru_{i+1}^{n+1}} + \boldsymbol{(1+2r)u_i^{n+1}} - \boldsymbol{ru_{i-1}^{n+1}} = \boldsymbol{ru_{i+1}^{n}} + \boldsymbol{(1-2r)u_i^{n}} + \boldsymbol{ru_{i-1}^{n}} \text{..... (3.12)}$$

where:

$r = \frac{D_c \Delta t}{2\Delta x^2}$

D_c: the diffusion coefficient at time t (m^2/s)

Δt: the time step (s)

Δx: the depth increment (m)

u_i^t: chloride level at time t and slice I (% wt. of concrete)

i: 1. . . ., I is the particular slice of concrete,

t: the time step in the initiation-to-corrosion period.

An example of a chloride model that uses the finite difference approach is Life-365.

3.2.1 Life-365 Model

Life-365 is a computer program for predicting the service life and life-cycle cost of reinforced concrete exposed to chlorides. It was developed by Bentz and Thomas in 2001, derived from publications in the concrete literature. The program and manual were later updated by Ehlen (2013) and released as Life-365^{TM} V2.2. The main feature of the more recent development of Life-365 is the incorporation of the ASTM C1556 Module, which allows the estimation of the diffusion coefficient and surface concentration to be calculated using laboratory and field data. The service life predicted by the model is defined as the sum of two periods: the initial period, which is defined as the time to the onset of corrosion, and the propagation period, which is defined as the time for corrosion to reach an unacceptable level. The initial period is the time it takes for a sufficient

amount of chloride ions to penetrate to the level of reinforcement and initiate corrosion. This period is predicted using Fick's second law of diffusion given by Equation 2.5.

As mentioned earlier, the chloride diffusion coefficient is found to be temperature-dependent. The influence of temperature on concrete diffusivity is taken into account in this model by applying the Arrhenius equation describing the rate of chemical reactions, as shown in Equation (3.13):

$$D(T) = D_{T_0}.\exp\left[\frac{E_a}{R}\left(\frac{1}{T_0}-\frac{1}{T}\right)\right] \quad \text{(3.13)}$$

where D_{T0} is the chloride diffusion coefficient at a reference temperature, T_0, E_a is the energy activation of the concrete, typical average value is estimated at 35000 J/mol, R is the universal gas constant, J/mol, T_0 is the reference temperature, usually the room temperature, *K*, and *T* is Temperature, K.

In chloride prediction models, Equation (3.13) is often used in conjunction with the time-dependent diffusion coefficient model given by Equation (3.2), as shown in Equation (3.14), (Luping 1996; Omer 2016):

$$D(t,T) = D_{28}\left(\frac{t_{28}}{t}\right)^{m}.\exp\left[\frac{E_a}{R}.\left(\frac{1}{T_{ref}}-\frac{1}{T}\right)\right] \quad \text{(3.14)}$$

Life-365 uses Equation (3.14) to account for time and temperature dependencies of diffusion coefficient where the value of D_a is modified at every time step. The model is designed to provide yearly temperature profiles based on the geographical location using a database compiled from meteorological data. Alternately, the user can apply the local temperature profile in terms of monthly average temperatures. The model selects the appropriate value for the surface

concentration and the time for the build-up to reach a maximum value, after which it remains constant, based on type of structure, geographic area, and exposure. However, the user can choose to input his/her own input data. For the chloride transport key input parameters (mainly the D_{28} and value of m), the model uses the mix design to estimate the values of these parameters.

In addition, the model considers the use of various strategies of corrosion inhibitors, including chemical corrosion inhibitors, membranes and sealers, epoxy-coated steel, and stainless steel. These strategies are made available in Life-365 to increase the service life of reinforced structures. The user can select the most cost-effective strategy for his/her own project. It should be noted that some of these corrosion inhibitors affect only the propagation period of corrosion and not the initial corrosion period.

In this thesis, the time-to-corrosion initiation of the reinforcement of the bridges in Lower and Upper Durham was estimated using the error function solution with both constant and time-dependent diffusion coefficients. Life-365 was also used to estimate the service life. The influence of the time-dependent diffusion coefficient and time-dependent surface concentration on the estimated service life was evaluated, and the service life of the bridge decks was calculated for the two cases. In the first case, it was assumed that a High Performance Concrete (HPC) mix design was used in the construction of the two bridges. In the second case, it was assumed that the bridges were constructed using a Normal Concrete (NC) mix design.

The high performance concrete mix design was evaluated in the laboratory where chloride profiles were projected for both acid-soluble chloride and water-soluble chloride using the bulk diffusion test. The chloride parameters of the two types of chlorides were evaluated. Field data and the

complete experimental testing program used to evaluate the HPC mixtures are provided in Chapter 4.

4 FIELD DATA AND EXPERIMENTAL PROGRAM

Two types of data were investigated in thesis: Field data and laboratory experimental data. The field data were collected for the cover thicknesses of the Lower and Upper Durham bridges in New Brunswick using the GPR technique. The laboratory data were collected by evaluating a high performance concrete mix design typically used in highway bridge deck construction in Nova Scotia. The HPC mix design was evaluated for slump, air content, compressive strength, and chloride penetration. A description of these two types of data collections is provided in this chapter.

4.1 Field Data

Two bridges located in Durham Bridge, New Brunswick, Canada, were scanned using a GPR technique to determine the actual cover thickness of the reinforced concrete deck in each bridge. The town of Durham Bridge is located approximately 25 km north of the provincial capital of Fredericton on New Brunswick Route 8. Locally, the two bridges are referred to as the Upper Durham bridge and the Lower Durham bridge. The Lower Durham bridge deck is a 200-mm reinforced concrete slab measuring approximately 10 m wide by 31.45 m long. The Upper Durham bridge deck is also a 200-mm reinforced concrete slab measuring approximately 10 mm wide by 38.99 m long. Unfortunately, no information is publically available regarding the type of concrete used in the construction of these two bridges.

4.1.1 Ground Penetrating Radar

Ground Penetrating Radar (GPR) was used to detect the actual cover depth of the concrete over the reinforcement. GPR is a non-destructive method that uses electromagnetic radiation in the microwave band (UHF/VHF frequencies) of the radio spectrum, and detects the reflected signals from subsurface structures. GPR is used in various applications, including road structure

assessment, concrete inspections, geological investigations, archaeology, rail bed inspection, mining, and bridge deck inspections (Hasan and Yazdani 2014). GPR has been widely used to find concrete cover and thickness of old and newly bridge decks. In this research, a Geophysical Survey System Inc. SIR-20 GPR controller was used with a ground-coupled 1500 MHz antenna was used to survey the bridge deck. This is a new generation of the GPR data acquisition systems. It combines a rugged, powerful data collection unit and a laptop with GSSI's Windows-based RADAN NT post-processing software for ease and flexible use. The SIR-20 allows the operator to collect data in single-line mode, making data processing quick and easy. The GPR type used in this research is shown in Figure 4.1.

Figure 4.1 GSSI SIR-20 GPR

4.1.2 GPR Technique

The GPR technique works by transmitting a very short electromagnetic pulse into the ground using a transmitter antenna. The abrupt changes in dielectric properties cause parts of the

electromagnetic energy to reflect back to the ground surface. Therefore, the pulse is reflected when meets various types of targets (rebar, voids, etc.) hidden in soil, pavement or any other medium. The reflected signal is collected and recorded by the GPR through a receiver antenna. The recorded signal is registered as amplitude and the GPR produces an image of the subsurface by using the two-way travel time and contrast in amplitude of initial and reflected signal (Hasan and Yazdani 2014; Mechbal and Khamlichi 2017).

The electromagnetic wave propagates in air with the speed of light (300 mm/ns). In other medium rather than air, the velocity of electromagnetic waves is different or reduced as it will be dependent on other factors. According to Moller and Vosgerau, 2005, the velocity of the electromagnetic waves is dependent on the relative dielectric permittivity, ε, the relative magnetic permeability, μ, and the electrical conductivity, σ. The velocity of electromagnetic waves in a host material is given by (Moller and Vosgerau 2005):

$$V = \frac{C}{\sqrt{\varepsilon\mu\frac{1+(\sigma/\omega\varepsilon)^2}{2}}} \quad \text{(4.1)}$$

Where C is the electromagnetic wave velocity or speed of light in vacuum (300 mm/ns), ε the dielectric permittivity of the medium and $\omega = 2\pi f$ the angular frequency, where f is frequency, and the expression $\sigma/\omega\varepsilon$ is a loss factor. In non-magnetic ($\mu = 1$) materials, such as a concrete, where $\sigma/\omega\varepsilon \approx 0$, the velocity of electromagnetic waves is reduced to the expression:

$$V = \frac{C}{\sqrt{\varepsilon_r}} \quad \text{(4.2)}$$

4.1.3 Factors Affecting The Dielectric Constant of Concrete

Researchers show that the dielectric constant of concrete is affected by several factors These factors include the moisture or water content, chloride ion concentration, hydration, temperature and the addition of supplementary cementious materials (Chen et al. 2012; Dérobert and Villain 2017; Dérobert et al. 2017; Xiao et al. 2017).

It has been found that an increase in both water content and chloride concentration in the pore solution can lead to significant decrease in the amplitude of both direct and reflected waves of the GPR. Therefore, the high water content and chloride ion concentration in the pore solution may result in inaccurate concrete dielectric permittivity constants (Dérobert and Villain 2017; Dérobert et al. 2017). Concrete cover with high water content can lead to an increase in the value of dielectric constant, which could result in over-prediction of the actual covers. This is mainly attributed to the increase in complex permittivity related to the polarization and conduction mechanisms occurring in concrete (Hasan and Yazdani 2014). Replacement of cement with supplementary cementious materials has been found to reduce the dielectric constant of concrete (Yehia et al. 2014). Hydration of concrete found also to affect wave velocity, signal travel time and real permittivity. As concrete hydrates, CSH formation will reduce the amount of free water in the matrix, thus, decreases the dielectric permittivity constant (Lai,W.L., Kind, T., Wiggenhauser, H. 2010). In addition, temperature has been found to significantly affect the real dielectric constant of concrete, especially at early ages (Chen et al. 2012). However, it seems that all these factors have marginal effects on dielectric properties of concrete when compared to the influence of the water content, porosity, and chloride content (Lai,W.L., Kind, T., Wiggenhauser, H. 2010; Nguyen, L.H.A., Beaucour, L., Ortola, S., Noumowé, A. 2014).

It must be, however, noted that in a high performance concrete such as that recently used in bridge decks, which is usually made with low w/c ratio and has low chloride ingress permeability and low porosity, the influence of many of the above factors can be limited on the estimate value of the relatively dielectric constant value. In this research the relative dielectric permittivity, ε, is estimated constant and taken to be equal to 7.5 for the investigated high performance concrete mix used in this research.

4.1.4 GPR Reflection Profiling

In reflection profiling mode the antennae are kept at constant separation distance, S, while they are moved along a profile. The electromagnetic pulses are transmitted at fixed time or distance interval. The signal is recorded and displayed immediately on a computer screen as GPR profiles, in which the vertical axis is two-way travel time in nanoseconds (ns) and the horizontal axis is distance along the measured profile. The GPR data are either collected along a single profile or in a grid of profiles to obtain 2D or pseudo 3D information on structures in the ground. The GPR data can also be acquired along lines so densely spaced that the line spacing equals the step size along the line. This leads to a 3D data cube, where data also can be displayed as time or depth slices (Neal 2004).

In this research, the GPR data were typically collected in the direction perpendicular to the upper rebar orientation. Therefore, since the upper rebar orientation is usually transverse, the data were collected in the direction of traffic. If the rebar orientation is unknown, it can easily be determined by acquiring sample GPR data in both directions and then comparing the arrival times of the rebar reflections in the data.

GPR data along each bridge was collected in parallel lines approximately 50 cm apart. Since the two bridges have the same width, 34 data files were collected in total for each bridge in lines parallel to the direction of the traffic, starting approximately 50 cm from the edge. Data were collected at a density of about 6 scans per 1 m. Following the data collection, the GPR data files were transferred from the SIR-20 to the laptop for processing and determination of the cover thickness in mm units.

4.1.5 Calculating The Cover Thickness Using The GPR

Figure 4.2 shows how the GPR is used to calculate the concrete cover thickness (distance from the concrete surface to the reinforcing bar surface). The GPR analysis software RADAN calculates the bar depth based on the time delay, t, measured from the data.

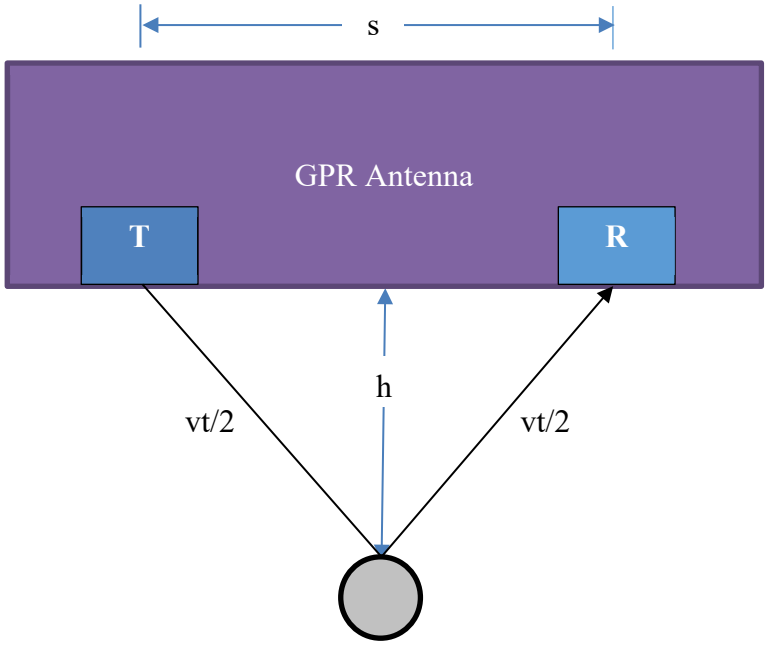

Figure 4.2 GPR Ray Diagram Schematic Shows How Thickness is Calculated

As can be seen from Figure 4.2, the GPR antenna consists of a transmitter, T, and a receiver, R, which are separated by some horizontal distance, S. S is equal to 58 mm for the 1500 MHz antenna.

The time delay that is measured from the collected data is assumed to be measured as the difference between the time the signal leaves the transmitter, travels down through the concrete, reflects off the rebar, travels back up through the concrete and is received at the receiver. While the GPR emits a field, which radiates outward from the transmitter, it is often assumed that the wave behaves like a single ray that travels along a straight-line pathway from T to the bar and back to R. This pathway is an isosceles triangle, with the side between T and R having a length of S, and the other two sides each having a length of v*t/2. The depth of the bar, h, is represented as a vertical line between the bar and the midpoint of S. The bar depth, h, is then calculated using the Pythagorean theorem for triangles:

$$h^2+\left(\frac{s}{2}\right)^2=\left(\frac{v*t}{2}\right)^2 \quad \text{..... (4.3)}$$

$$h=\sqrt{\left(\frac{v*t}{2}\right)^2-\left(\frac{s}{2}\right)^2} \quad \text{.....(4.4)}$$

Normally, the actual depth is measured from a core sample over a couple of bars where t has been measure in order to calibrate the actual velocity of the GPR signal. The GPR signal was found to be sensitive to the moisture content and moisture gradient of the concrete cover. Therefore, the results may vary a bit, depending on the moisture content and how it changes versus depth into the concrete, so there is usually some variability in the estimate. However, assuming the relative dielectric constant to be 7.5 is a decent estimate of what someone might expect for concrete.

4.2 Laboratory Experimental Data

The high performance concrete mix design was tested to determine its chloride transport properties and parameters. The projected chloride parameters were determined using the bulk diffusion test, as per ASTM C1556. Two types of chloride profiles – water-soluble chloride profiles and acid-soluble chloride profiles – were established and projected. The chloride parameters for each type were determined using the error function solution as per the ASTM C1556 standard test method. The concrete mix design details, sample preparation and description of the laboratory test method are provided in the following sections.

4.2.1 Concrete Mix Design

The concrete mix design tested in this project is given in Table 4.1. The concrete is made with ternary blended cement contained 5% silica fume and 25% ground granulated blast furnace slag as a partial replacement of Portland cement.

Table 4.1 Concrete Mix Design and Proportions

Lafarge Tercem (kg/m^3)	**Water (kg/m^3)**	**W/C**	**Sand (kg/m^3)**	**20 mm Coarse Aggregate (kg/m3)**	**AEA (ml/m^3)**	**HRWR (ml/m^3)**	**Retarder (ml/m^3)**
435	140	0.32	740	1060	1500	2500	1000

The chemical and physical analyses of the blended cement used in the high performance concrete mixture are presented in Table 4.2.

Table 4.2 Cement Chemical and Physical Properties

Chemical Analysis			**Physical Analysis**		
Item	**Spec. Limit**	**Test Results**	**Item**	**Spec. Limit**	**Test Results**
SiO_2 (%)	-	27.2	Blaine fineness (m^2/kg)	-	568
Al_2O_3 (%)	-	6.4			
Fe_2O_3 (%)	-	1.81		76 min	98.2

CaO (%)	-	51	Fineness, res. passing on 45 um		
MgO (%)	5.0 max	4	Fineness, res. retained on 45 um	24 max	1.8
Sulphate as SO_3 (%)	3.0 max	4.18			

4.2.2 Casting and Preparation of Concrete Samples

A ready concrete mix truck supplied the concrete to the lab site. As soon as the concrete arrived, slump and air content tests were performed as per ASTM C143 and ASTM C231, respectively, followed by casting of the concrete testing cylinders. Two sizes of cylinders were prepared and cast: small standard cylinders with a dimension of 100 mm in diameter and 200 mm in height, and larger cylinders with a dimension of 150 mm in diameter and 300 mm in height. A vibrating table was used to consolidate the cast cylinders. Twenty-four hours later, the cylinders were demolded and stored for 28 days in a standard moisture room. The smaller cylinders were used for the compressive strength test and other tests, and the larger cylinders were used for the bulk diffusion test to obtain both water-soluble and acid-soluble chloride profiles. A photo of the prepared cylinders is shown in Figure 4.3.

Figure 4.3 Concrete cylinders prepared and cast in the laboratory

4.2.3 Compressive Strength Test

Three standard test cylinders after 28 days of curing were tested for compressive strength in accordance with ASTM C 39. Prior to the testing, the specimens were capped in accordance with ASTM C 617. The testing machine used in this study is the Furney Testing Machine Model F-40, with a capacity of about 250,000 lb, as shown in Figure 4.4. The compressive strength of each specimen was calculated in accordance with the ASTM C 39 analysis procedure.

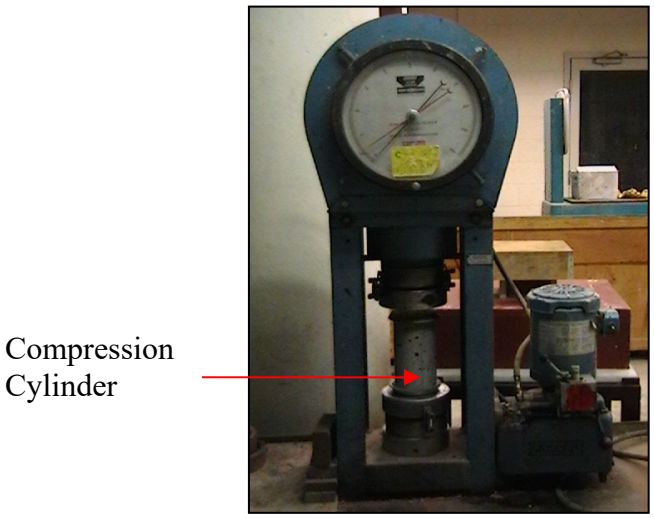

Figure 4.4 Compression testing machine

4.2.4 Bulk Diffusion Test (ASTM C1556 - 11a)

The bulk diffusion test was conducted as per ASTM C1556-11a to obtain the chloride concentration profiles. The larger cylinders were cored and cut to produce smaller cylinders with dimensions coinciding with those recommended by the standard. All cored specimens were 100 mm in diameter and 75 mm in height, and were side-coated (except for the exposed surfaces) using a thin continuous layer of an impermeable 2-part epoxy called Concresive Paste, so the chloride is allowed to penetrate through the surface only, as shown in Figure 4.5. The sealed specimens were then immersed in a calcium hydroxide solution for 24 hours at 23 ± 2° C prior to immersion in a chloride solution to avoid the effect of capillary suction that may take place when the specimens are first exposed to the chloride solution. Afterwards, the specimens were immersed in a chloride solution with a concentration of 165g/l at room temperature for three periods of exposure: 56, 90 and 180 days.

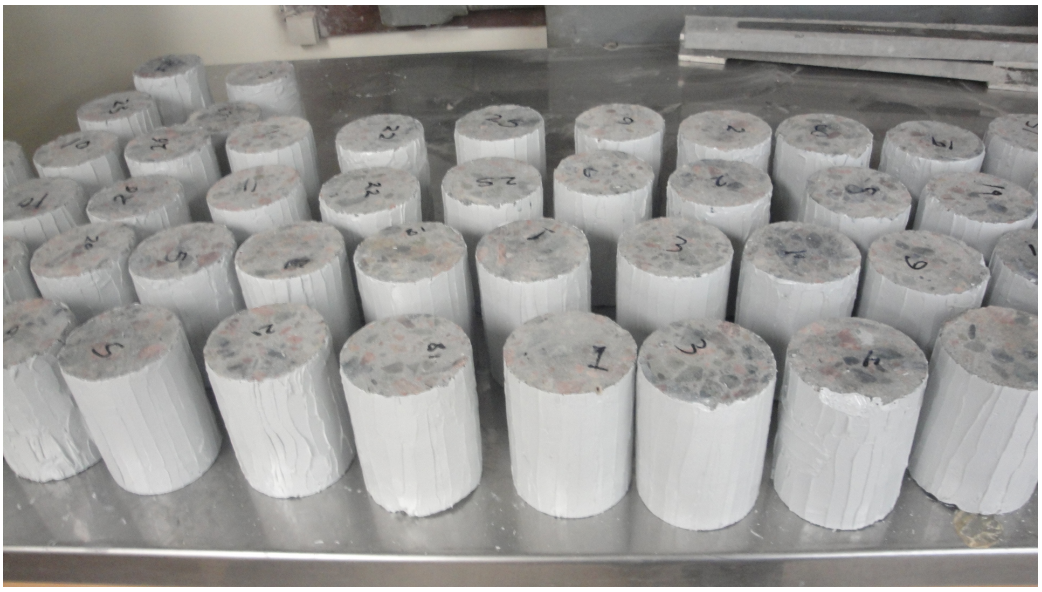

Figure 4.5 Concrete samples prepared as per ASTM C1556 for the chloride diffusion test

At the end of each exposure period, the specimens were removed, washed with water, and left to dry in the laboratory air environment. Prior to grinding, the epoxy coating layer around the test specimen close to the exposed surface was removed to maintain the pure concrete depth of the specimen and to avoid any contamination from the coating material. Then the test specimens were ground in l mm layer thickness parallel to the exposed surface, using the milling machine shown in Figure 4.6.

For specimens immersed for 56 days, 10 layers of powder were obtained up to 10 mm depth from the surface. However, for specimens immersed for 90 and 180 days, 20 layers were obtained up to 20 mm depth from the exposed surface. Each powder sample layer weighed between 10 and 13 g. The collected powder of each layer was then analyzed for acid-soluble chloride content, as per ASTM C1152, and for water-soluble content, as per ASTM C1218.

Figure 4.6 Milling machine used to grind-test concrete specimens

The chloride content from each layer was determined using the METTLER TOLEDO T50 titrator shown in Figure 4.7. Three samples of each layer were titrated to determine the chloride concentration and the average was calculated. Once the average chloride content was calculated for all layers in the samples, the chloride concentration of each layer was plotted against its corresponding depth to obtain the chloride profiles. Three acid-soluble and three water-soluble chloride profiles were obtained from the concrete specimens for each exposure period.

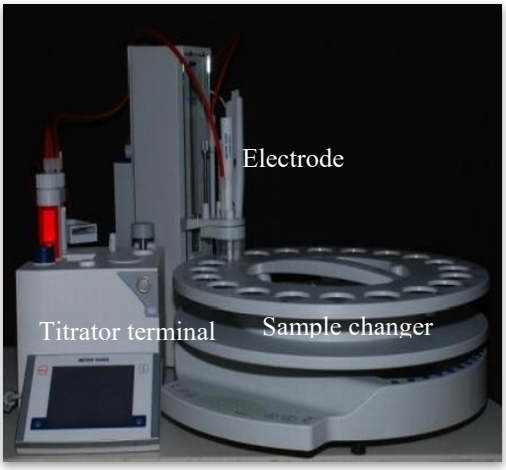

Figure 4.7 METTLER TOLEDO T50 Titrator equipment

5 RESULTS AND DISCUSSION

This chapter presents the results of the field and laboratory investigation data. The field data include the GPR collected data for the Upper and Lower Durham bridges. The laboratory data and results include the laboratory test results of the high performance concrete mixture typically used in the construction of bridge decking in Nova Scotia. The determination of chloride parameters is provided. The time-to-corrosion initiation (service life) is calculated using the error function solution and finite difference (Life-365) models. The influences of time, temperature, and surface concentration dependencies on the p

redicted service life are discussed.

5.1 Field Data Results

Figure 5.1 shows the GPR image of one of the bridges. The image shows the details of the deck structure, including the location and thickness of the asphalt layer, concrete cover thickness, and location of the upper and lower reinforcements. The area, which exhibited weak reflection amplitude, is indicative of deterioration. These weak reflections can be the result of elevated chloride content, concrete degradation, or corrosion of reinforcing steel rebar, all of which attenuate the radar signal.

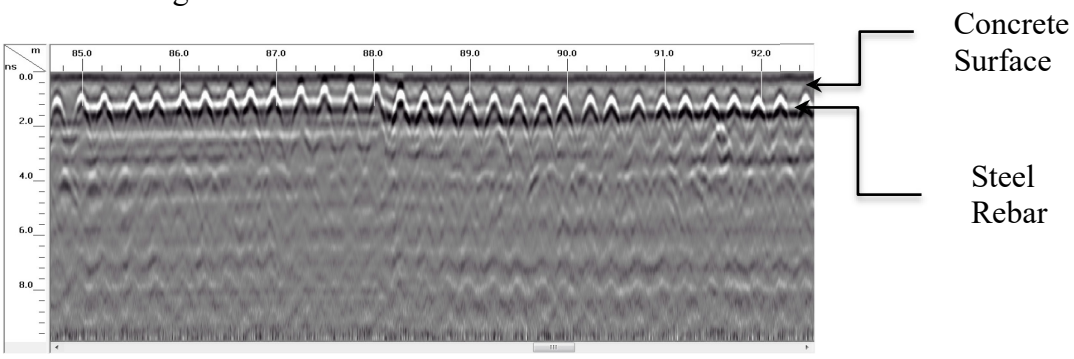

Figure 5.1 GPR image showing details of bridge deck structure

The cover thickness data resulting from the field measurements using the GPR for each bridge are presented in the following subsections.

5.1.1 Upper Durham Bridge

Figures 5.2 and 5.3 show the histogram and image of cover thickness for the Upper Durham bridge deck, respectively. Both were created using the GPR collected data. The histogram shows the various cover thickness plotted against the their number of its frequencies (data points). As can be seen in Figure 5.3, the GPR collected data reveal large variations in the cover thickness of the reinforced concrete deck. In some areas, the deck has very shallow cover thickness (40 mm or less), while in other areas the cover thickness was a quite thick (above 100 mm). The range of variation in the cover thickness is higher than that specified by CAN/CSA-S6 standard (70 ± 20 mm).

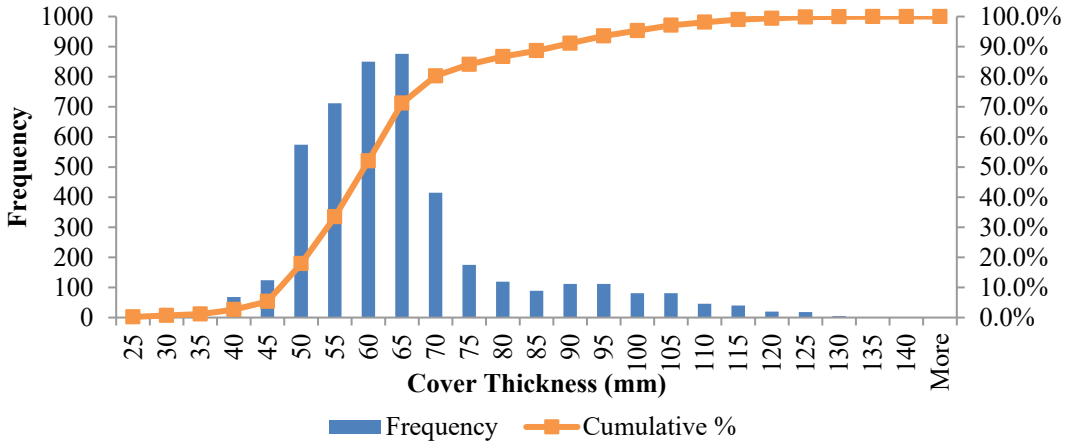

Figure 5.2 Histogram of cover thickness based on GPR data - Upper Durham Bridge

However, the majority of the bridge deck area exhibited a satisfactory cover thicknesses fall within the specified range. The dominated cover thickness of this bridge deck was 65 mm. Such a large

variation in the measured cover thickness can have a significant effect on the calculated service life as will be seen later in this Chapter.

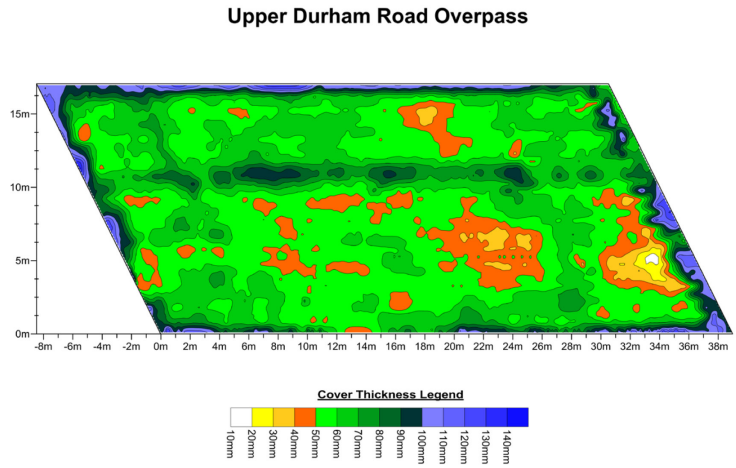

Figure 5.3 GPR image of Upper Durham Bridge deck

5.1.2 Lower Durham Bridge

For the Lower Durham Bridge, the measured cover thickness was similar to that of the Upper Durham Bridge. However, the cover depth variation is relatively lower, as shown in Figure 5.4.

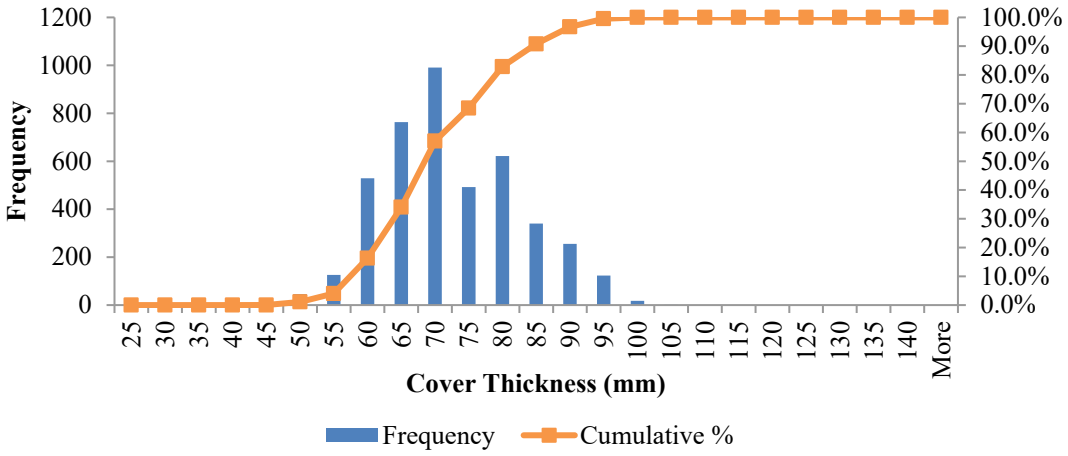

Figure 5.4 Histogram of cover thickness based on GPR data - Lower Durham Bridge

The cover thicknesses of this bridge ranged from 55 mm and 95 mm. Also, the dominated cover thickness (70 mm) is slightly higher than that of Upper Durham Bridge (65 mm). Figure 5.5 shows the GPR collected data graphically. From this figure, it is clear that the majority areas of the two bridge decks do comply with the minimum cover thickness requirements as specified by CAN/CSA-S6-06 of Canadian Highway Bridge Code, which is 70 ± 20 mm for concrete cast-in-place. However, the shallow areas of Upper Durham Bridge deck with 40 mm cover depth or less will corrode quickly and in a relatively short period of time compared to those with a deeper cover thickness, which might lead to early corrosion intitation of the bridge deck.

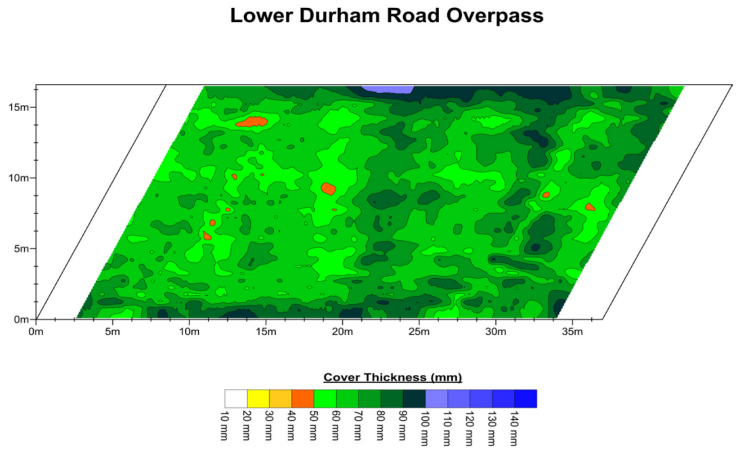

Figure 5.5 GPR image for Lower Durham Bridge deck

This is because the time it takes for chloride ions to penetrate and accumulate at the level of the reinforcement will be very short compared to that of a deeper cover thickness, where it will take longer time to the reach the reinforcing steel level. The detected cover thickness data obtained via GPR will be used in the life prediction models to calculate the time-to-corrosion initiation for the

two bridges. The influence of cover thickness on the predicted service life of the two bridges will be discussed in greater detail later in this chapter.

5.2 Laboratory Concrete Data and Results

The results of the high performance concrete mixture investigated in this research are provided in the following subsections. These results include slump, air content, compressive strength, and water-soluble/acid-soluble chloride profiles.

5.2.1 Slump and Air Content Test Results

The concrete mixture was workable and easy to handle. The mixture had a slump of 110 mm and air content of 8%. The air content was within the specified range (6% – 8%) as per CSA A23.1 for concrete exposed to freeze-and-thaw action.

5.2.2 Compressive Strength Test Results

The results of the compressive strength are presented in Table 5.1. As expected, the low w/c ratio and the incorporation of 5% silica fume by mass as a partial replacement of Portland cement has led to a relatively high 28-day compressive strength.

Table 5.1 Compressive Strength Results

Concrete Cylinder No.	Compressive Strength (MPa)	Average Compressive Strength (MPa)
1	61.20	59.5
2	58.20	
3	59.10	

5.2.3 Bulk Diffusion Test Results

In this section, the results of the bulk diffusion test are presented. Both water-soluble chloride profiles and acid-soluble chloride profiles were established. The acid-soluble chloride profiles

represent the total chloride concentration (e.g., both free and bond chlorides), whereas the water-soluble chloride profiles represent only the chloride concentration in the pore solution (e.g., free chloride concentration).

5.2.3.1 Water-soluble Chloride Profiles

The water-soluble chloride profiles obtained at 56, 90 and 180 days are illustrated in Figure 5.6. It should be noted that the chloride concentration of the first layer (first millimeter from the surface) was discarded, as recommended by the test standard. The average chloride profiles for the three periods of exposure are plotted together, as shown in Figure 5.7. As it can be seen, the chloride concentration decreases as the depth of the concrete increases.

Figure 5.7 shows that the chloride concentration at any given depth increases as the time of exposure increases, except for the chloride concentration close to the exposed surface for the 180-day specimen, which is slightly lower than that of the 90-day one. This could be the result of the heterogeneous distribution of the paste and coarse aggregate close to the surface of the concrete specimens.

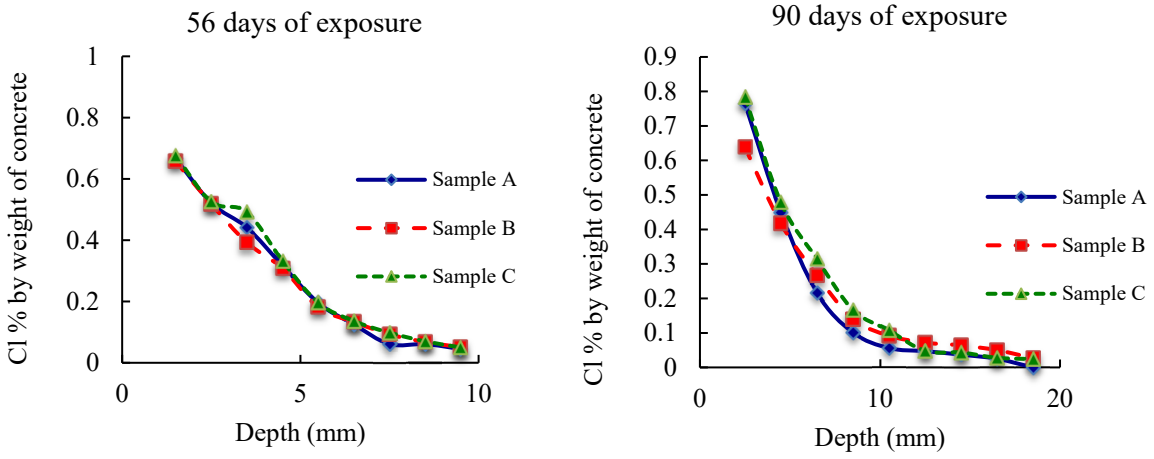

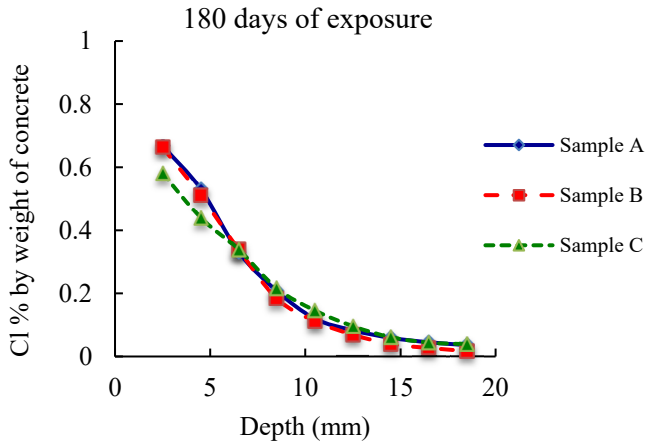

Figure 5.6 Experimental water-soluble chloride profiles at different periods of exposure

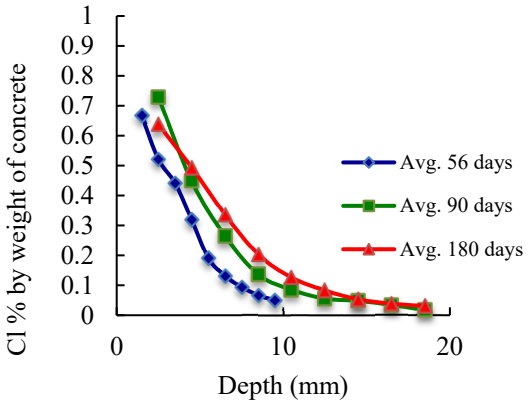

Figure 5.7 Average experimental water-soluble chloride profiles at 56, 90 and 180 days of exposure

5.2.3.2 Acid-soluble Chloride Profiles

Similarly, the acid-soluble chloride concentrations of different layers were plotted against their corresponding depths for the three exposure periods shown in Figure 5.8. As can be seen, the results of the three specimens for each exposure period are very consistent through all depths except for close to the surface, where some discrepancies in the chloride concentrations among the concrete specimens were noted. The average chloride profiles for the three periods were plotted

together, as shown in Figure 5.7. Like the case of the water-soluble chloride, the acid-soluble chloride concentration increases as the length of exposure increases.

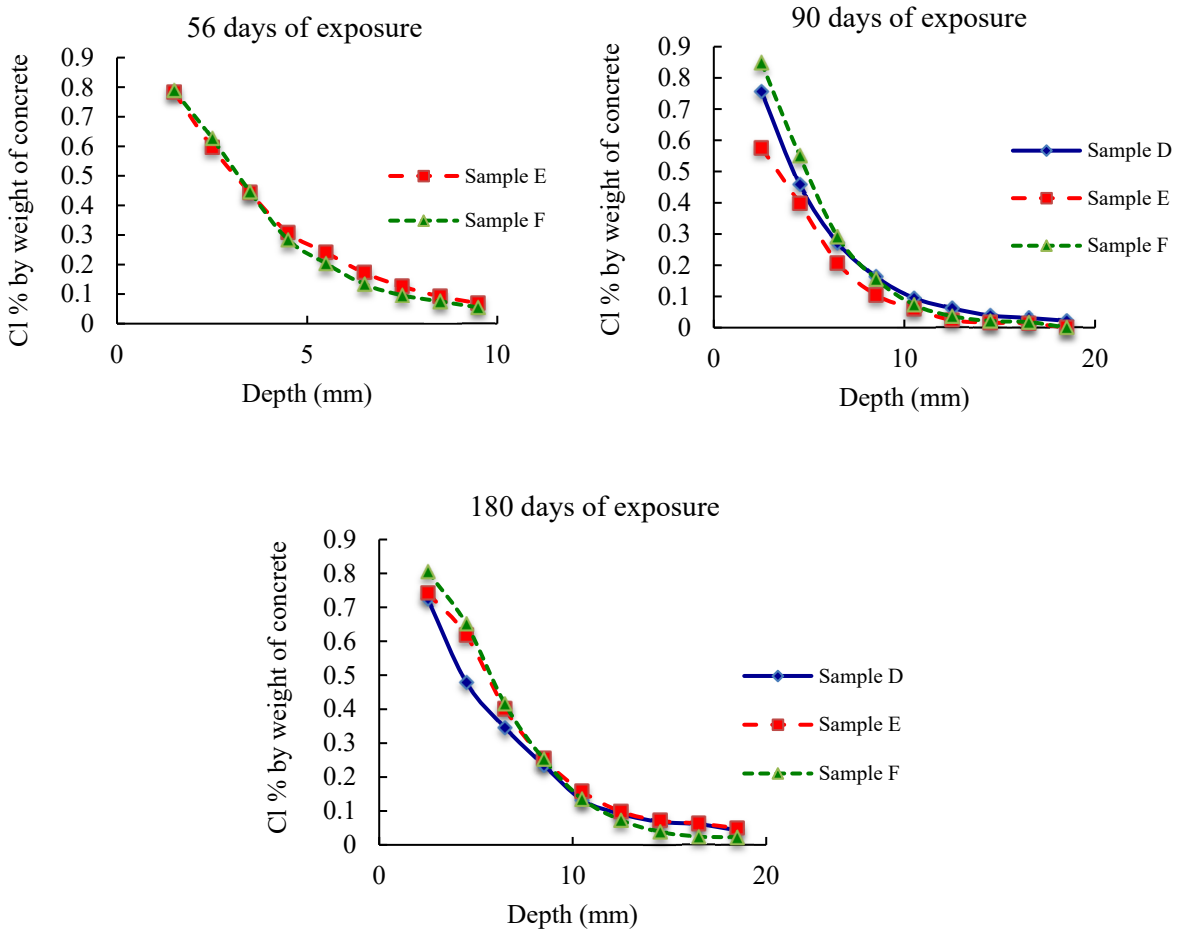

Figure 5.8 Experimental acid-soluble chloride profiles at different periods of exposure

Figures 5.8 and 5.9 clearly show that the acid-soluble chloride concentration is higher than that of water-soluble (Figures 5.2 and 5.4) at all depths and is also more pronounced for depths close to the surface. This was expected, as the acid-soluble chlorides represent the total chloride content (both bound and free chloride concentrations), while the water-soluble chlorides are believed to represent only the free chloride concentrations in the pore solution.

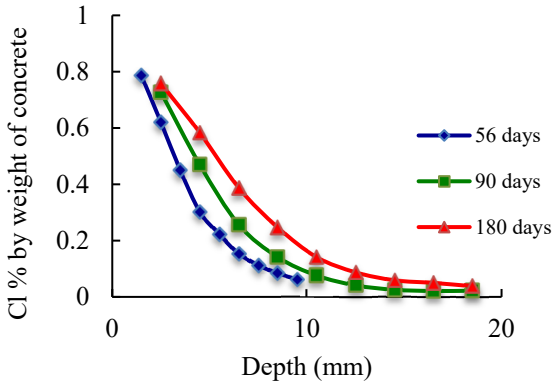

Figure 5.9 Average experimental acid-soluble chloride profiles at 56, 90 and 180 days of exposure

Several researchers believe that water-soluble may over estimate the amount of free chloride concentration in the pore solution by allowing the loosely bond chlorides to dissolve in the pore solution during the extraction process (Glass et al. 1996; Sandberg 1995). Furthermore, the heat generated from the milling process may cause some chemically bound chlorides to release in the pore solution, which leads to an increase in the amount of free chlorides.

5.2.4 Determination of Chloride Parameters

5.2.4.1 Determination of Average Diffusion Coefficient and Surface Concentration (Constant Values)

The average chloride diffusion coefficient, D_a and the surface chloride concentration C_s, are determined for each exposure period by fitting the error function solution (shown in Equation 5.1) to the corresponding average experimental chloride profiles of both water-soluble and acid-soluble chlorides using nonlinear analysis of the least squared method.

$$C(x,t) = C_s - (C_s - C_i).\text{erfc}\left(\frac{x}{2\sqrt{D.t}}\right), \qquad x > 0,\ t > 0 \qquad \text{.....(5.1)}$$

where C_i is the background chloride.

Figures 5.10 and 5.11 shows the error function solution profiles (modeled profiles) as fitted to the experimental chloride profiles of water-soluble and acid-soluble chlorides, respectively.

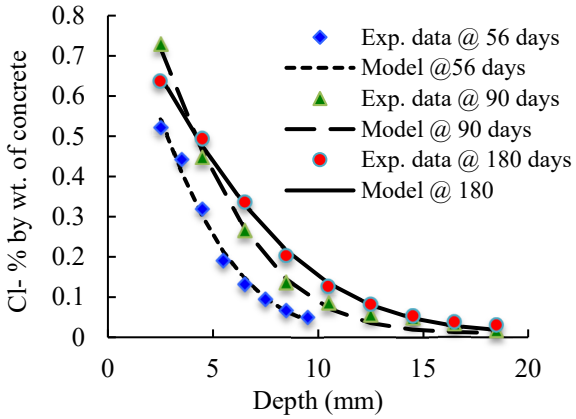

Figure 5.10 Error function solution and experimental water-soluble chloride profiles for three exposure periods

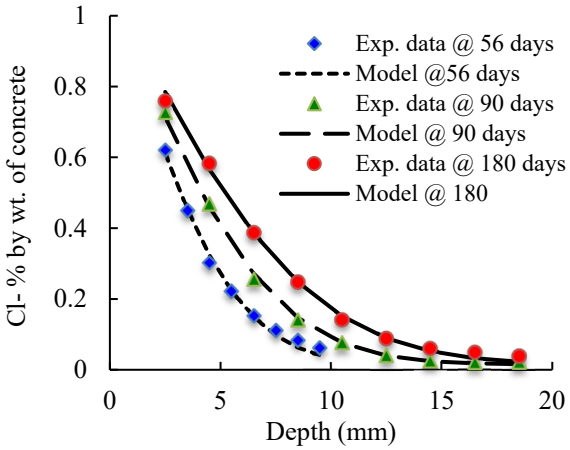

Figure 5.11 Error function solution and experimental acid-soluble chloride profiles for three exposure periods

The average diffusion coefficients and surface chloride concentrations resulting from the fitting process for both water-soluble and acid-soluble chlorides are summarized in Table 5.2.

Table 5.2 Water-soluble and Acid-soluble Chloride Parameters of HPC

Exposure Period (days)	Water-soluble Chloride		Acid-soluble Chloride	
	C_s (%)	$D_{AVG}*10^{-12}$ (m^2/s)	C_s (%)	$D_{AVG}*10^{-12}$ (m^2/s)
56	0.932	2.08	1.076	1.89
90	1.102	1.95	1.131	1.84
180	0.89	1.64	1.063	1.58

5.2.4.2 Determination of Time-dependent Diffusion Parameters (m and D_{28})

As discussed in section 3.1.2, there are three determination techniques reported in the literature for calculating the value of m and the instantaneous diffusion coefficient. These techniques are total time method, average time method and effective time method, and were used to obtain the values for the time-dependent diffusion parameters. The values of D_{avg} obtained by fitting the error function solution to the experimental water-soluble and acid-soluble, shown in Table 5.2, were plotted against the three calculated times: t_{tot}, t_{avg} and t_{eff} on a log – log scale. A linear regression was then applied to the plotted data. The value of m is determined as the slop of the best-fit regression line, as shown in Figures 5.12 and 5.13 for water-soluble and acid-soluble chlorides, respectively.

It is interesting to see how the value of m (i.e., the slop of the best-fit of the regression line) changes as the time plotted for each technique changes. This shows that the value of m is highly dependent on the representative time used. Different methods resulting in different representative times lead to different values of m. It can also be seen that the effective time technique resulted in the highest value of m, while the total time method led to the lowest value of m. These results stand in very good agreement with those presented by Nokken et al. (Nokken et al. 2006)

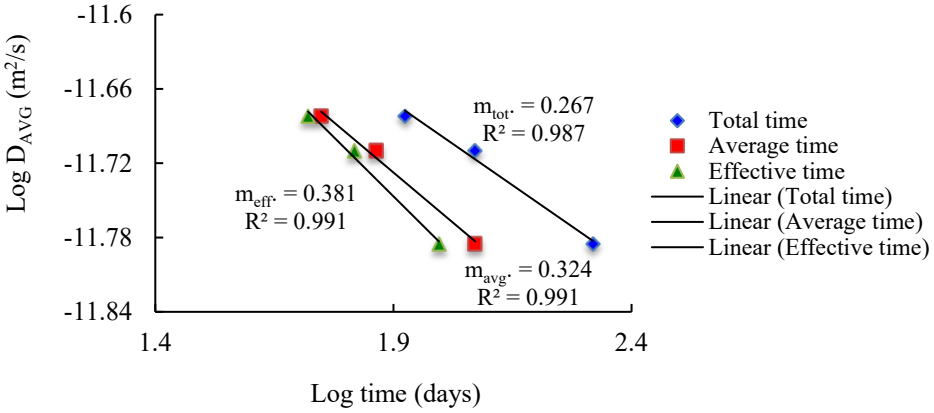

Figure 5.12 Determination of m using three time representative techniques (based on water-soluble results)

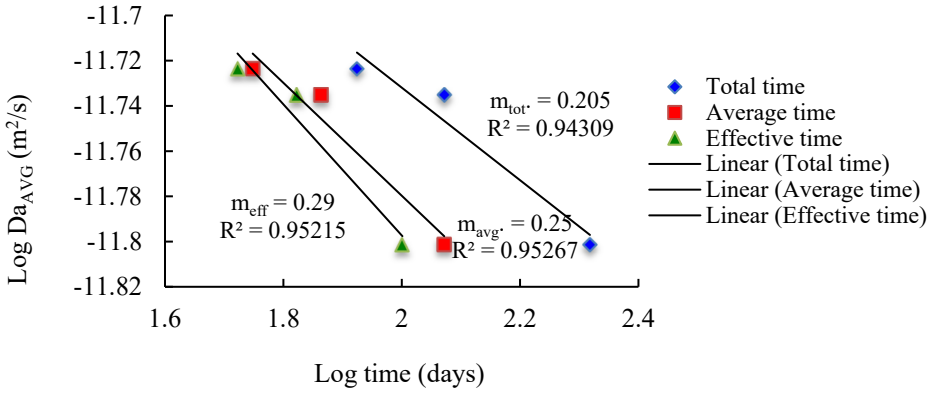

Figure 5.13 Determination of m using three time representative techniques (based on acid-soluble results)

The value of D_{28} is determined from Equation (3.2) using the value of m and the 1-day diffusion coefficient. The one-day diffusion coefficient is determined as the intercept of the regression line with y-axis. The resulting values of m and D_{28} days are summarized in Table 5.3. It can be seen that the value of D_{28} changes slightly as the value of m changes. This implies that the time method used to calculate the value of m has insignificant influence on the value of D_{28}.

Table 5.3 Time-dependent Diffusion Parameters of HPC

Water-soluble Chloride.						**Acid-soluble Chloride**					
$D_{28}*10^{-12}$ (m^2/s)	**$m_{tot.}$**	**$D_{28}*10^{-12}$ (m^2/s)**	**m_{avg}**	**$D_{28}*10^{-12}$ (m^2/s)**	**$m_{eff.}$**	**$D_{28}*10^{-12}$ (m^2/s)**	**$m_{tot.}$**	**$D_{28}*10^{-12}$ (m^2/s)**	**m_{avg}**	**$D_{28}*10^{-12}$ (m^2/s)**	**$m_{eff.}$**
2.81	0.27	2.63	0.32	2.68	0.381	2.41	0.21	2.28	0.25	2.31	0.29

The value of m can have significant influence on the predicted service life. The lower values of m will lead to more conservative life predictions, whereas the higher values will result in less conservative time-to-corrosion initiation, as will be seen in the following section.

By comparing the results of water-soluble chloride to that of acid-soluble chloride in Tables 5.2 and 5.3, it can be seen that the surface concentrations of acid-soluble chloride are higher than those of water-soluble chlorides for the three exposure periods. However, the chloride diffusion coefficients of water-soluble chloride are higher than those of acid-soluble chloride. This shows a kind of correlation between the surface concentration and the diffusion coefficient. The higher the surface concentration is, the lower the diffusion coefficient, and vice-versa. For the value of m, the acid-soluble chloride resulted in lower values compared to those for water-soluble chloride, which exhibited slightly higher values of m.

5.3 Service Life Predictions

In this thesis, the service life of the two bridge decks was calculated as the time-to-corrosion initiation by chloride ions using the error function solution and finite difference model (Life-365). The concrete transport properties (chloride parameters) of the acid-soluble chloride were used in the calculation of the service life. Both error functions with constant and time-dependent diffusion coefficients were used. Life-365 was used with constant and time-dependent surface

concentrations. Different values of m, as determined from three techniques, were used in the time-dependent error function solution to examine the influence of each parameter on the predicted service life. The influence of different cover thicknesses on the time-to-corrosion initiation was evaluated and assessed.

Because the mix designs of the two bridge decks were unknown, it was assumed that the reinforced concrete deck was constructed using two different concrete mixtures. First, it was assumed that the two decks were constructed using the high performance concrete mix design evaluated in this research. The second assumption was that the two decks were constructed using a normal concrete mix design. For the purpose of this research, the chloride transport properties of a normal concrete mix design evaluated by Thomas and Bamforth (Thomas and Bamforth 1999) were used in the service life calculations. The normal concrete mixture was made with a 0.4 w/c ratio and contained Portland cement only. The mixture has the following transport properties: constant diffusion coefficient, D_a = 9.5 x 10^{-12} m^2/s measured after one year of exposure, instantaneous diffusion coefficient, D_{28} = 8 x 10^{-12} m^2/s and value of m = 0.14 (Thomas and Bamforth 1999). In addition, the following assumptions were used in the chloride models for the purpose of service life estimations of the two decks:

- A maximum surface chloride concentration, C_{smax} = 1. 0% by weight of concrete,
- Chloride background, C_i = 0.00 % by weight of concrete
- Chloride threshold value, C_{crit} = 0.05% by weight of concrete.
- 60 mm cover thickness.

For the error function model, the service life of the high performance concrete was calculated for the following cases:

- Constant D_a at 56, 90 and 180 days using the error function solution shown in Equation (3.1)
- Time-dependent diffusion coefficient as per m_{tot}, m_{avg} and m_{eff}. The time-to-corrosion initiation was calculated using the error function solution shown in Equation (3.4).

The results of the time-to-corrosion initiation resulting from the different chloride models are tabulated in Table 5.4 and graphically illustrated in Figure 5.14.

Table 5.4 Estimation of Service Life Based on Error Function Solution (Years)

Cover Thickness (mm)	**Based on Constant Diffusion Coefficient (D_{AVG})**				**Based on Time-dependent Diffusion Coefficient (D_{28})**			
	HPC			NC	HPC			NC
	Da_{56}	Da_{90}	Da_{180}	Da_{180}	m_{tot}	m_{avg}	m_{eff}	m
60	8	8	9	1.5	16	22	28	2.6

Figure 5.12 shows that the constant diffusion coefficient (average diffusion coefficient) led to very conservative service life estimations, whereas the time-dependent diffusion coefficient resulted in less conservative ones.

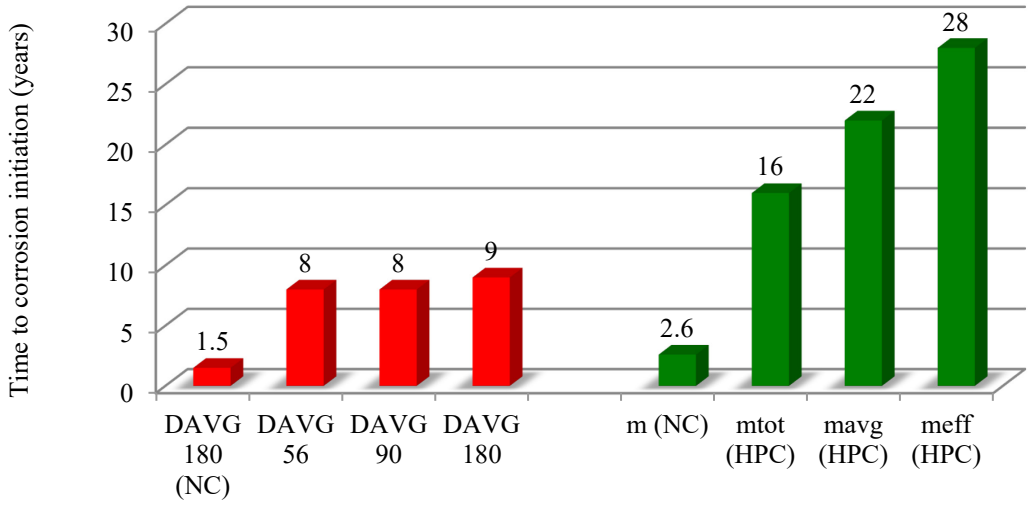

Figure 5.14 Service life estimation based on error function solution with constant and time-diffusion coefficients

Figure 5.14 indicates that the average diffusion coefficients obtained based on exposure periods ranged from 56 to 180 day has little to no influence on the time-to-corrosion initiation. The three diffusion coefficients resulted in almost similar numbers of years, with a slight increase for the 180-day value. By comparing these results to those of the time-dependent diffusion coefficient, it can be seen that the reduction of diffusion coefficient with time has a significant impact on time-to-corrosion predictions. Thus, depending on the value of m used in the prediction, the service life can be as high as almost three times of that determined based on constant diffusion value. On the other hand, the influence of the value of m is shown to have a strong impact on the time-to-corrosion initiation. While the m_{tot} resulted in the lowest time-to-corrosion initiation, the m_{eff} exhibited the highest number of years for corrosion initiation. The m_{avg} resulted in a corrosion initiation time that is between the two. This is implies the high sensitivity of the estimated service

life to the used value of m. It also implies the importance of proposing a standard test method for the determination of the value of m.

Figure 5.14 also indicates that that the high performance concrete mixture provided much higher service life compared to that of normal concrete in both cases of diffusion coefficients. This shows the durability advantage of the high performance concrete mixture over the normal concrete, particularly when the time-dependent diffusion coefficient is considered. The lower values of diffusion coefficients at age 28 days for the HPC concrete mix design mainly contributed to the low w/c ratio and the presence of 5% silica fume by mass, while the ongoing reduction in the diffusivity over time is mostly attributed to the incorporation of 25% of slag by mass, which continues to hydrate over a longer period of time.

The service life as predicted from the time-dependent error function solution model was also compared to that resulting from Life-365. Life-365 estimates the chloride parameters based on the mix design of the concrete mixtures. For the purpose of comparison, the temperature in Life-365 was kept constant at 20 ^{o}C. The surface concentration was also kept constant during the exposure in both models. The chloride transport parameters for both the high performance concrete and normal concrete mixtures as estimated by Life-365 are given in Table 5.5. The time-to-corrosion initiation as estimated by Life-365 and the time-dependent error function solution model is compared in Figure 5.15.

Table 5.5 Chloride Parameters and Service Life Estimations as Predicted by Life-365

Concrete Mixture Type	**D_{28} (m^2/s)**	**m**	**Time-to-corrosion Initiation (years)**
NC	13.8×10^{-12}	0.20	1.7
HPC	2.24×10^{-12}	034	33

As can be seen in Table 5.5, both the D_{28} value and m, as estimated by Life-365 for NC concrete mixtures, are higher than those determined by Thomas and Bamforth (Thomas and Bamforth 1999). Similarly, Life-365 estimates higher D_{28} and m values than those estimated in this research for the HPC concrete mixture. As a result, the Life-365 resulted in time-to-corrosion initiation that is higher than that resulting from the time-dependent error function solution for the HPC mix design. However, it resulted in a lower time-to-corrosion initiation for the NC mix design. The time-effective method exhibited service life estimation close to that resulting from Life-365. This may indicate that the time-effective approach as proposed by Stanish and Thomas (Stanish and Thomas 2003) is likely more accurate for the estimation of D_{28} and value of m.

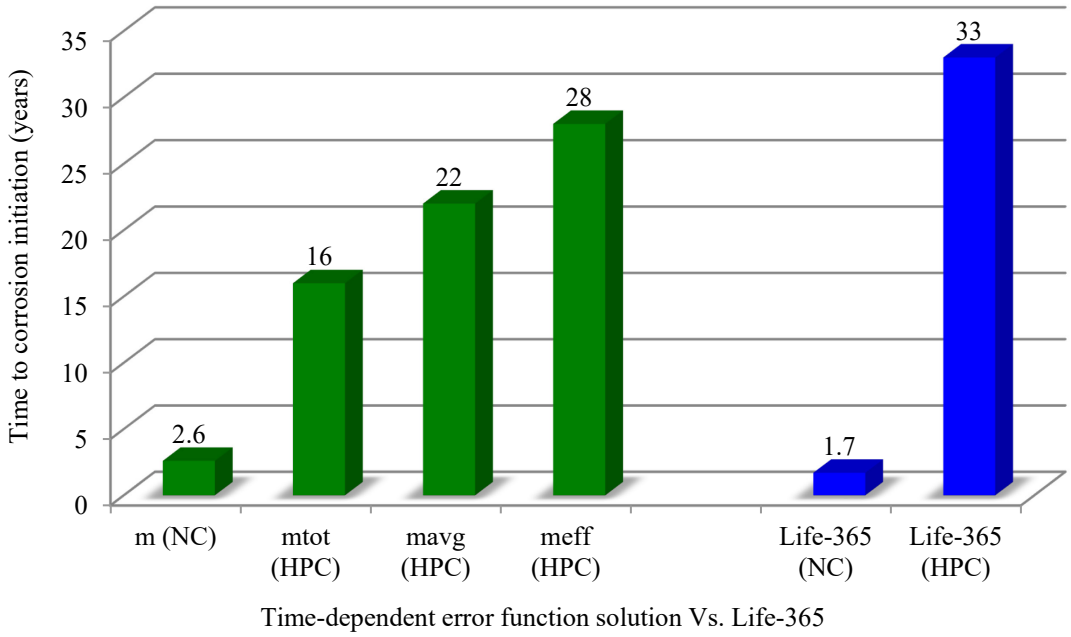

Figure 5.15 Service life estimations (time-dependent error function solution Vs. Life-365)

5.3.1 Influence of Time-dependent Surface Concentration on Estimated Service Life

The influence of the time-dependent surface concentration was evaluated in this thesis using Life-365 for the HPC concrete mixture. Two cases were considered: a constant maximum surface chloride concentration of 1.0%, and time-dependent surface concentration where the surface concentration built up linearly from 0 up to the maximum of 1.0% during the first 8 years of exposure, beyond which it was assumed to be constant up to the end of the service life. The influence of the time-dependent surface concentration on the estimated service life is shown in Figure 5.16.

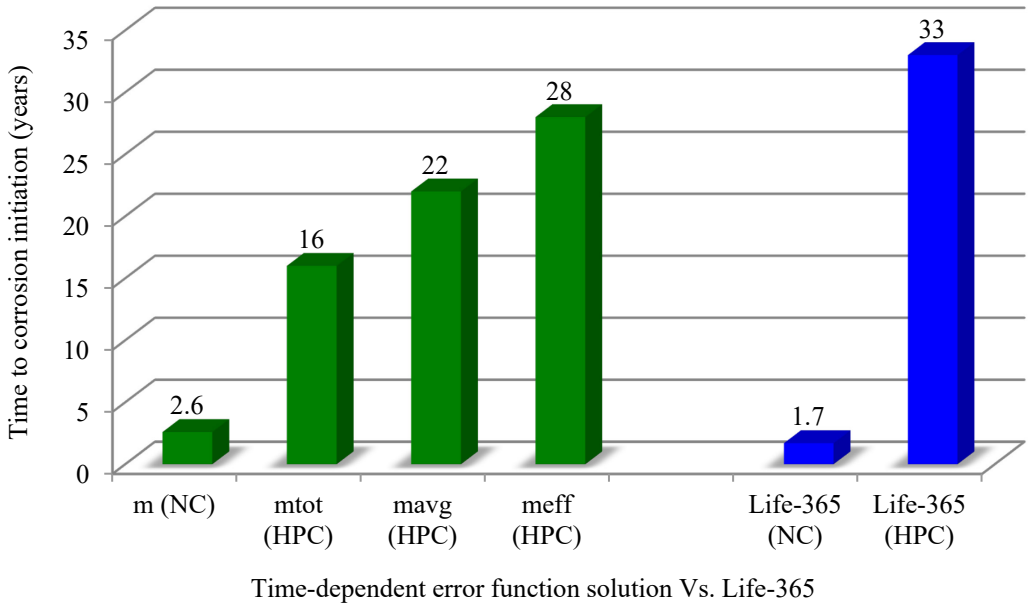

Figure 5.16 Influence of time-dependent surface concentration on service life estimation

As can be seen, when the surface concentration was taken as time-dependent, the service life of the structure increased by approximately 23%. This shows the importance of including the time-dependent surface concentration in the prediction models for proper estimation of service life.

5.3.2 Influence of Cover Thickness on Service Life Estimation

To evaluate the influence of concrete cover thickness on the predicted service life, the measured cover depths collected using GPR technique were used. It was assumed that both bridge decks were made of HPC concrete mixture. The service life was calculated using HPC concrete mixture evaluated in the lab and had the following chloride transport properties: D_{a28} = 2.31 x 10^{-12} m^2/s; m_{eff} = 0.29, and C_s = 1%. The results were plotted using histogram charts as shown in Figure 5.16 and 5.17 for Upper and lower Durham bridge decks, respectively.

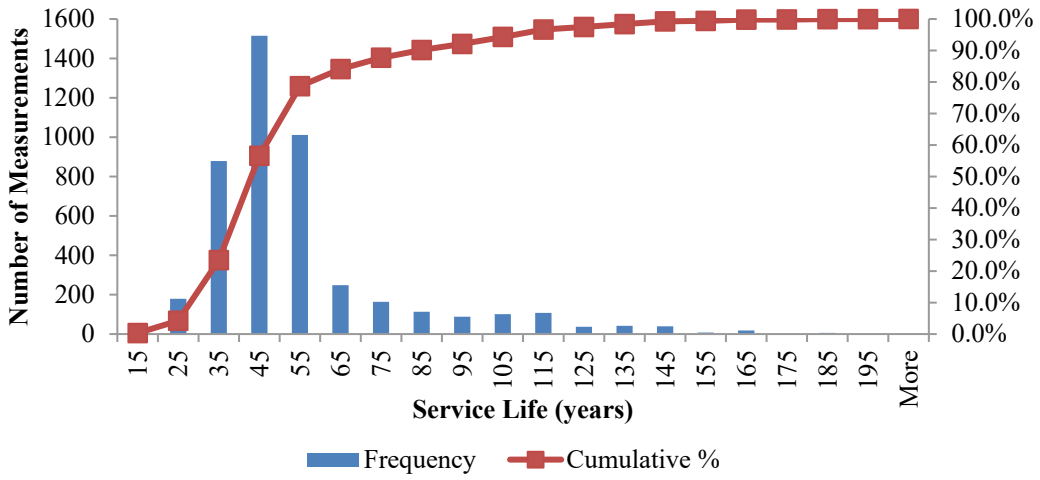

Figure 5.17 Service life predictions based on measured cover thickness - Upper Durham Bridge

As can be seen from Figure 5.17 the cover thickness of the Upper Durham bridge deck, the predicted service life varies significantly from location to location of the bridge deck. It depends on the measured conver thickness at the specific loacation. Shallow cover thicknesses (e.g., <40 mm) resulted in lower number of years (25 years). Therefore, areas with unsuficient cover thickness will start to corred first and the time to corrosion inintiation increases as the cover thickness increases. For this bridge the majorty of the surface exhpted service life of 45 to 55 years.

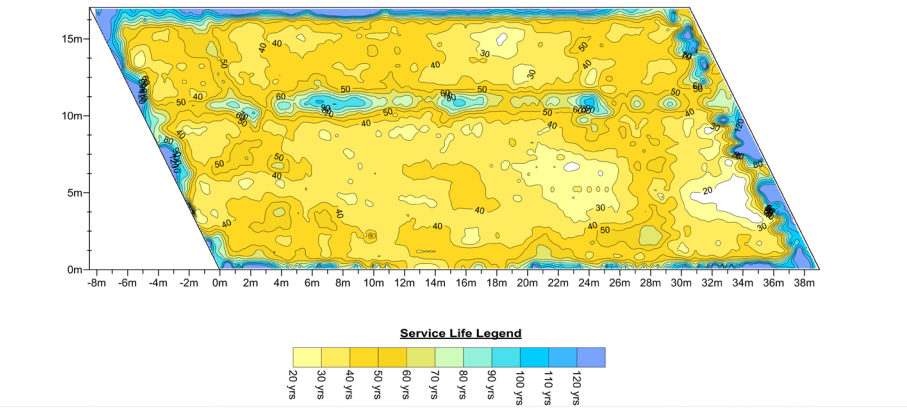

Figure 5.18 Upper Durham Road Overpass

Similar variation in the predicted service life is also observed for Lower Durham Bridge deck, as shown in Figures 5.19 and 5.20 . However, large portion of the deck surface exhpted slightly higher service life than that of Upper Durham Bridge deck. This is because the average cover thickness was slightly higher for Lower Durham Bridge compared to that of Upper Durham Bridge.

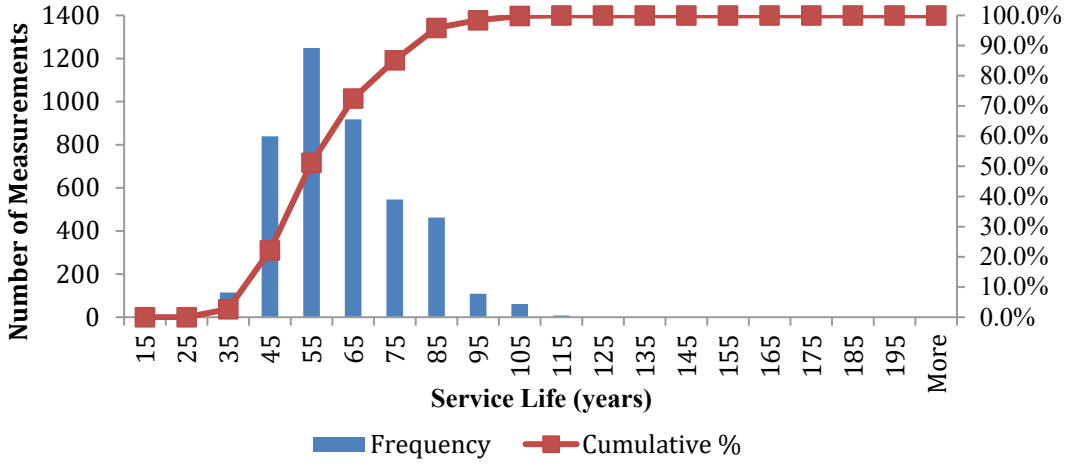

Figure 5.19 Service life predictions based on measured cover thickness - Lower Durham Bridge

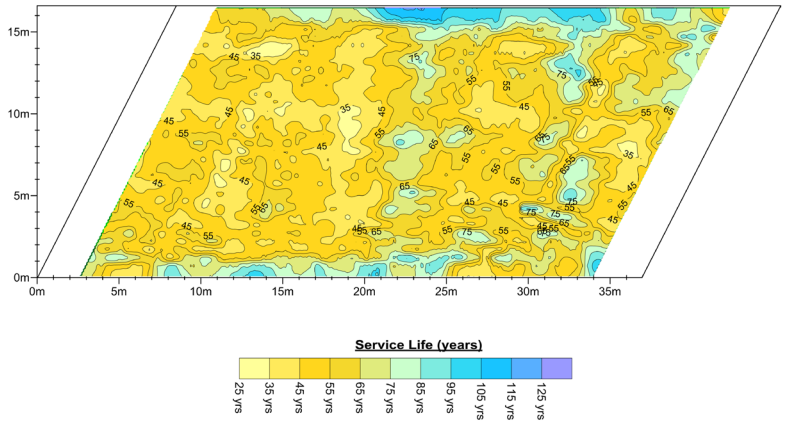

Figure 5.20 Lower Durham Road Overpass

The large veriation in the covere thickness of the two bridge decks attributed to the larage variation in the applied cover thickness. This shows the importance of constrcution practices in applying approperiate cover thickness over the reinforcement. It's very interesting to note that, the cover thickness can play a significant role in determineing the time to corrosion initation and therefore can control the time when the repair/maintenance is needed. Because once a part of the bridge deck starts to corroed (i.e., with the least conver thickness) it can propegate and spread out very quickly.

According to Karlsson and Poulsen (Karlsson, M. and Poulsen, E 1995), the time at which the repair should take place can be determined based on a probabilistic approach. Since the reinforcing steel of the bridge will start to corrode at different times due to the variations in cover thickness (which is the control factor in this case), the service life can be defined by the time at which a certain level of corrosion (e.g., 10% of the bridge area) has started to appear.

6 CONCLUSIONS AND FUTURE WORK

6.1 Conclusions

Based on the work carried out in this research, the following conclusions can be drawn:

- The GPR collected data revealed significant variations in the cover thickness of the Lower and Upper Durham bridges. The shallowest cover thickness was 15 mm and the deepest was 120 mm. These significant variations have led to major differences in the predicted service life of the two reinforced concrete decks. However, the majority of the bridge surface area in the Lower Durham bridge has an average cover thickness of 60 mm, while that in the Upper Durham bridge has an average core thickness of 50 mm.

- The High Performance Concrete (HPC) mixture evaluated in this research resulted in substantially higher service life compared to that of the Normal Concrete (NC) mixture.

- No significant differences have been found in the chloride parameters between water-soluble and acid-soluble chlorides. However, the chloride diffusion coefficients projected from acid-soluble chloride were slightly lower than those projected based on water-soluble chloride measurements.

- The average diffusion coefficient values resulted in unrealistic and very conservative service life. This may indicate the invalidity of using the average diffusion coefficient as determined by the bulk diffusion in providing reasonable service life predictions.

- The three time techniques used in the determination of the value of m resulted in different values of m. The effective time method resulted in the highest value of m and the total time method resulted in the lowest.

- The cover thickness has a notable influence on the time-to-corrosion initiation. Shallow cover thickness resulted in very short time-to-corrosion initiation, while deep cover thickness led to a significant increase in the estimated time-to-corrosion initiation.

- The estimated service life was found to be greatly influenced by the projected value of m, the time-dependent diffusion coefficient, and the time-dependent surface concentrations.

6.2 Future Work

- Further work and research is needed to determine which time method is more appropriate for the determination of the age parameter (m).

- In this thesis, the service life was modeled based on the assumption that chloride ions transport solely by a diffusion process which takes place in fully saturated concrete. Further research is needed to consider the influence of other chloride transport mechanisms, such as convection or capillary absorption, which takes place in partially dry concrete.

REFERENCES

Ahmad, S. (2003). "Reinforcement corrosion in concrete structures, its monitoring and service life prediction—a review." *Cement and Concrete Composites,* 25(4–5), 459-471.

Aït Mokhtar, K., Loche, J-M. Friedmann, H. Amiri, O. Ammar A. (2007). "Concrete in marine environment - Steel corrosion in reinforced concrete ." *Rep. No. Report n°2-2,* .

Amey, S. L., Johnson, D. A., Miltenberger, M. A., and Farzam, H. (1998). "Predicting the service life of concrete marine structures: An environmental methodology." *ACI Struct.J.,* 95(2), 205-214.

Andrade, C., Diez, J. M., and Alonso, C. (1997). "Mathematical modeling of a concrete surface `skin effect' on diffusion in chloride contaminated media." *Adv.Cem.Based Mater.,* 6(2), 39-44.

Angst, U., Elsener, B., Larsen, C. K., and Vennesland, O. (2009). "Critical chloride content in reinforced concrete - A review." *Cem.Concr.Res.,* 39(12), 1122-1138.

Ann, K. Y., Ahn, J. H., and Ryou, J. S. (2009). "The importance of chloride content at the concrete surface in assessing the time to corrosion of steel in concrete structures." *Constr.Build.Mater.,* 23(1), 239-245.

Arya, C., Buenfeld, N. R., and Newman, J. B. (1990). "Factors influencing chloride-binding in concrete." *Cem.Concr.Res.,* 20(2), 291-300.

Bamforth, P. (1996). "Predicting the risk of reinforcement corrosion in marine structures." *Corros.Prev.Control,* 43(4), 91-100.

Bentur, A., Diamond, S., & Berke. (1997). *Steel corrosion in concrete: Fundamentals and civil engineering practice.* E & FN Spon, London.

Bjegovic, D., Stirmer, N., and Serdar, M. (2012). "Durability properties of concrete with blended cements." Wiley-VCH Verlag, P.O. Box 101161, Weinheim, D-69451, Germany, 1087-1096.

Boddy, A., Bentz, E., Thomas, M. D. A., and Hooton, R. D. (1999). "Overview and sensitivity study of a multimechanistic chloride transport model." *Cem.Concr.Res.,* 29(6), 827-837.

Bouikni, A., Swamy, R. N., and Bali, A. (2009). "Durability properties of concrete containing 50% and 65% slag." *Constr.Build.Mater.,* 23(8), 2836-2845.

Burris, L. E., and Riding, K. A. (2014). "Diffusivity of binary and ternary concrete mixture blends." *ACI Mater.J.,* 111(4), 373-382.

Byfors, K. (1987). "Influence of silica fume and fly ash on chloride diffusion and pH values in cement paste." *Cem.Concr.Res.,* 17(1), 115-130.

Byfors, K. (1986). "Chloride binding in cement paste." *Nordic Concrete Research,* (5), 27-38.

Chalee, W., and Jaturapitakkul, C. (2009). "Effects of W/B ratios and fly ash finenesses on chloride diffusion coefficient of concrete in marine environment." *Materials and Structures/Materiaux Et Constructions,* 42(4), 505-514.

Chen, W., Shen, P., and Shui, Z. (2012). "Determination of water content in fresh concrete mix based on relative dielectric constant measurement." *Construction and Building Materials,* 34 306-312.

Chen, Y., Chiu, H., Chan, Y., Chang, Y., and Yang, C. (2013). "The correlation between air-borne salt and chlorides cumulated on concrete surface in the marine atmosphere zone in North Taiwan." *Journal of Marine Science and Technology (Taiwan),* 21(1), 24-34.

Dérobert, X., Lataste, J. F., Balayssac, J. -., and Laurens, S. (2017). "Evaluation of chloride contamination in concrete using electromagnetic non-destructive testing methods." *NDT & E International,* 89 19-29.

Dérobert, X., and Villain, G. (2017). "Effect of water and chloride contents and carbonation on the electromagnetic characterization of concretes on the GPR frequency band through designs of experiment." *NDT & E International,* 92 187-198.

Fredriksen, J. M., Mejlbro, L., and Nilsson, L. O. (2008). "Fick's 2nd law-Complete solution for chloride ingress into concrete with focus on time dependent diffusivity and boundary condition." *Rep. No. TVBM-3146,* .

Glass, G. K., Wang, Y., and Buenfeld, N. R. (1996). "Investigation of experimental methods used to determine free and total chloride contents." *Cem.Concr.Res.,* 26(9), 1443-1449.

Hasan, M. I., and Yazdani, N. (2014). "Ground penetrating radar utilization in exploring inadequate concrete covers in a new bridge deck." *Case Studies in Construction Materials,* 1 104-114.

Hausman D.A.,. (1967). "Steel corrosion in concrete." *Material Protection,* 6(11) 19-22.

Ipavec, A., Vuk, T., Gabrovek, R., and Kaucic, V. (2013). "Chloride binding into hydrated blended cements: The influence of limestone and alkalinity." *Cem.Concr.Res.,* 48 74-85.

Jones, M. R., Dhir, R. K., and Magee, B. J. (1997). "Concrete containing ternary blended binders: Resistance to chloride ingress and carbonation." *Cem.Concr.Res.,* 27(6), 825-831.

Karlsson, M. and Poulsen, E. (1995). "Design of rebar concrete covers in marine concrete structures – probabilistic approach." *RILEM Workshop, StRemy-les-Chevreuse,* .

L. Tang, H. E. Sørensen. (2001). "Precision of the Nordic test methods for measuring the chloride diffusion/migration coefficients of concrete." *Materials and Structures, RILEM Publications SARL,* 34 479 - 485.

Lai,W.L., Kind, T., Wiggenhauser, H. (2010). "A study of concrete hydration and dielectric relaxation mechanism using ground penetrating radar and short-time Fourier transform." *EURASIP J Adv Signal Process,* 2010 1-14.

Long, A. E., Henderson, G. D., and Montgomery, F. R. (2001). "Why assess the properties of near-surface concrete?" *Constr.Build.Mater.,* 15(2-3), 65-79.

Luping, T. (1996). "Chloride transport in concrete - measurement and prediction." *PhD Thesis, Doktorsavh.Chalmers.Tek.Hogsk.,* (1245),.

Luping, T., and Gulikers, J. (2007). "On the mathematics of time-dependent apparent chloride diffusion coefficient in concrete." *Cem.Concr.Res.,* 37(4), 589-595.

Luping, T., and Nilsson, L. (1993). "Chloride binding capacity and binding isotherms of OPC pastes and mortars." *Cem.Concr.Res.,* 23(2), 247-253.

Luping, T., and Nilsson, L. (1992). "Chloride diffusivity in high strength concrete at different ages." *Nordic Concrete Research,* (11), 162-162.

Maage, M., Helland, S., Poulsen, E., Vennesland, O., and Carlsen, J. E. (1996). "Service life prediction of existing concrete structures exposed to marine environment." *ACI Mater.J.,* 93(6), 602-608.

Mangat, P. S. and Molloy, B. T. (1994). "Prediction of long term chloride concentration in concrete." *Materials and Structures,* 27 338 - 346.

Martin-Perez, B., Zibara, H., Hooton, R. D., and Thomas, M. D. A. (2000). "Study of the effect of chloride binding on service life predictions." *Cem.Concr.Res.,* 30(8), 1215-1223.

Mechbal, Z., and Khamlichi, A. (2017). "Determination of concrete rebars characteristics by enhanced post-processing of GPR scan raw data." *NDT & E International,* 89 30-39.

Mehta, P., and Monteiro, J. M. (2006). *Concrete: Microstructure, Properties, and Materials.* McGraw-Hill Professional, .

Mehta, P. K. (1991). *Concrete in the marine environment.* Elsevier Applied Science, London; New York.

Mejlbro, L. (1996). "The Complete Solution to Fick's 2nd Law of Diffusion with Time-Dependent Diffusion Coefficient and Surface Concentration." .

Moller, I., and Vosgerau, H. (2005). "Testing ground penetrating radar for resolving facies architecture changes – a radar stratigraphic and sedimentological analysis along a 30 km profile on the Karup Outwash Plain." Near Surface Geophysics, Denmark.

Murthi, P., and Sivakumar, V. (2008). "Strength-porosity relationship for ternary blended concrete." *Indian Concrete J.,* 82(7), 35-41.

Neal, A. (2004). "Ground-penetrating radar and its use in sedimentology: principles, problems and progress." *Earth-Science Reviews,* Earth-Science Reviews, 66:261-330.

Neville, A. M. (1996). *Properties of Concrete.* J. Wiley, New York.

Nguyen, L.H.A., Beaucour, L., Ortola, S., Noumowé, A. (2014). "In fluence of the volume fraction and the nature of fine lightweight aggregates on the thermal and mechanism properties of structural concrete
." *Concrete Build Materials,* 51 121 - 132.

Nilsson, L. O., Poulson, E., Sandberg, P., Sorensen, H. E., Klinghoffer, O., and Fredriksen, J. M. (1996). "HETEK Chloride penetration into concrete, state-of- the-Art, transport processes, corrosion initiation, test methods and prediction models." *Rep. No. vol. 53, .*

Nilsson, L. (2009). "Models for chloride ingress into concrete - From Collepardi to today." *International Journal of Modelling, Identification and Control,* 7(2), 129-134.

Nokken, M., Boddy, A., Hooton, R. D., and Thomas, M. D. A. (2006). "Time dependent diffusion in concrete-three laboratory studies." *Cem.Concr.Res.,* 36(1), 200-207.

Omer, A. (2016). "Development of nonlinear finit difference model For chloride diffusion in concrete".

Omer, A., Barnes, C., and Newhook, J. (2015). "Effect of time and curing temperatures on chloride migration coeefficient and age parameter." *Annual Conference of the Canadian Society for Civil Engineering 2014: Sustainable Municipalities, May 28, 2014 - May 31,* Canadian Society for Civil Engineering, Halifax, NS, Canada, 1478-1487.

Page, C. L., Short, N. R., and El Tarras, A. (1981). "Diffusion of chloride ions in hardened cement pastes." *Cem.Concr.Res.,* 11(3), 395-406.

Pavlik, Z., Pavlikova, M., Fiala, L., Beneova, H., Mihulka, J., and Cerny, R. (2010). "Effect of slag on chloride transport and storage properties of HPC." *6th International Conference on Concrete under Severe Conditions-Environment and Loading, CONSEC'10, June 7, 2010 - June 9,* CRC Press, Merida, Yucatan, Mexico, 1497-1504.

Poulsen, E. (1993). "On a model of chloride ingress into concrete having time dependent diffusion coefficient." *Nordic Miniseminar on Chloride Penetration into Concrete,* 1 - 12.

Poulsen, Ervin.,Mejlbro, Leif.,. (2006). *Diffusion of chloride in concrete : theory and application.* Taylor & Francis, London; New York.

Riding, K. A., Thomas, M. D. A., and Folliard, K. J. (2013). "Apparent diffusivity model for concrete containing supplementary cementitious materials." *ACI Mater.J.,* 110(6), 705-713.

Sandberg, P. (1995). "Critical Evaluation of Factors Affecting Chloride-Initiated Reinforcement Corrosion in Concrete." *Rep. No. TVBM-7088,* Division of Building Materials, Lund Institute of Technology, Sweden.

Shi, X., Xie, N., Fortune, K., and Gong, J. (2012). "Durability of steel reinforced concrete in chloride environments: An overview." *Constr.Build.Mater.,* 30(0), 125-138.

Song, H., Shim, H., Petcherdchoo, A., and Park, S. (2009). "Service life prediction of repaired concrete structures under chloride environment using finite difference method." *Cement and Concrete Composites,* 31(2), 120-127.

Song, L., Sun, W., and Gao, J. (2012). "Effect of W/B to the time dependent chloride diffusion in concrete with GGBS." *2nd International Conference on Civil Engineering, Architecture and Building Materials, CEABM 2012, May 25, 2012 - May 27,* Trans Tech Publications, Yantai, China, 144-147.

Song, Q., Shen, B., and Zhou, Z. (2011). "Effect of blast furnace slag and steel slag on cement strength, pore structure and autoclave expansion." *2011 International Conference on Structures and Building Materials, ICSBM 2011, January 7, 2011 - January 9,* Trans Tech Publications, Guangzhou, China, 17-20.

Stanish, K.D., Hooton, R.D., and Thomas, M.D.A. (1997). "Testing the chloride penetration resistance of concrete: A literature review." .

Stanish, K., and Thomas, M. (2003). "The use of bulk diffusion tests to establish time-dependent concrete chloride diffusion coefficients." *Cem.Concr.Res.,* 33(1), 55-62.

Status of the Nations Highways and Bridges. (July 2, 1991). "Conditions, performance, and capital Investment requirements." .

Takewaka, K. and Mastumoto, S. (1988). "Quality and cover thickness of concrete based on the estimation of chloride penetration in marine environments." *ACI SP 109-17,* 109 381-400.

Thomas, M. D. A., Hooton, R. D., Scott, A., and Zibara, H. (2012). "The effect of supplementary cementitious materials on chloride binding in hardened cement paste." *Cem.Concr.Res.,* 42(1), 1-7.

Thomas, M. D. A., Shehata, M. H., Shashiprakash, S. G., Hopkins, D. S., and Cail, K. (1999). "Use of ternary cementitious systems containing silica fume and fly ash in concrete." *Cem.Concr.Res.,* 29(8), 1207-1214.

Thomas, M. D. A., and Bamforth, P. B. (1999). "Modelling chloride diffusion in concrete effect of fly ash and slag." *Cem.Concr.Res.,* 29(4), 487-495.

Xiao, X., Ihamouten, A., Villain, G., and Dérobert, X. (2017). "Use of electromagnetic two-layer wave-guided propagation in the GPR frequency range to characterize water transfer in concrete." *NDT & E International,* 86 164-174.

Yehia, S., Qaddoumi, N., Farrag, S., and Hamzeh, L. (2014). "Investigation of concrete mix variations and environmental conditions on defect detection ability using GPR." *NDT & E International,* 65 35-46.

Zibara, H. (2001). "Binding of External Chlorides by Cement Pastes, Ph.D. dissertation, Univ. of Toronto, Toronto, Ontario, Canada." .

APPENDIX A: Chloride Profiles

Water-soluble Test Results: solution temperature 22.4° C

56 days of exposure

Depth (mm)	Chloride concentration per sample (% by weight of concrete)			
	A	B	C	Avg.
0.5	0.954	1.051	1.008	1.004
1.5	0.667	0.658	0.676	0.667
2.5	0.521	0.518	0.525	0.521
3.5	0.441	0.392	0.492	0.442
4.5	0.317	0.308	0.332	0.319
5.5	0.195	0.181	0.196	0.191
6.5	0.125	0.133	0.136	0.131
7.5	0.061	0.093	0.098	0.094
8.5	0.061	0.068	0.07	0.066
9.5	0.045	0.051	0.05	0.049

90 days of exposure

Depth (mm)	Chloride concentration per sample (% by weight of concrete)			
	A	B	C	Avg.
0.5	1.109	1.124	0.976	1.070
2.5	0.765	0.638	0.784	0.729
4.5	0.449	0.417	0.478	0.448
6.5	0.216	0.266	0.314	0.265
8.5	0.101	0.14	0.167	0.136
10.5	0.056	0.092	0.107	0.085
12.5	0.047	0.072	0.048	0.056
14.5	0.037	0.064	0.043	0.048
16.5	0.025	0.05	0.028	0.034
18.5	0	0.027	0.024	0.017

180 days of exposure

Depth (mm)	Chloride concentration per sample (% by weight of concrete)			
	A	B	C	Avg.
0.5	0.925	1.188	0.767	0.960
2.5	0.668	0.663	0.581	0.637
4.5	0.531	0.51	0.44	0.494
6.5	0.331	0.339	0.339	0.336
8.5	0.208	0.184	0.216	0.203
10.5	0.12	0.112	0.146	0.126
12.5	0.083	0.069	0.096	0.083
14.5	0.059	0.039	0.061	0.053
16.5	0.045	0.027	0.044	0.039
18.5	0.036	0.017	0.039	0.031

Acid-soluble Test Results: solution temperature 22.4° C

56 days of exposure

Depth (mm)	Chloride concentration per sample (% by weight of concrete)			
	D	E	F	Avg.
0.5	0.901	0.976	0.956	0.944
1.5	0.786	0.783	0.789	0.786
2.5	0.637	0.596	0.627	0.620
3.5	0.459	0.443	0.446	0.449
4.5	0.316	0.307	0.283	0.302
5.5	-	0.24	0.203	0.222
6.5	-	0.172	0.133	0.153
7.5	-	0.126	0.096	0.111
8.5	-	0.092	0.075	0.084
9.5	-	0.069	0.055	0.062

90 days of exposure

Depth (mm)	Chloride concentration per sample (% by weight of concrete)			
	D	E	F	Avg.
0.5	1.242	0.829	1.408	1.160
2.5	0.756	0.576	0.849	0.727
4.5	0.458	0.398	0.551	0.469
6.5	0.272	0.207	0.291	0.257
8.5	0.163	0.105	0.156	0.141
10.5	0.095	0.06	0.073	0.076
12.5	0.062	0.024	0.037	0.041

14.5	0.039	0.016	0.021	0.025
16.5	0.031	0.014	0.018	0.021
18.5	0.022	0	0	0.022

180days of exposure

Depth (mm)	**Chloride concentration per sample (% by weight of concrete)**			
	D	**E**	**F**	**Avg.**
0.5	0.852	1.124	1.046	1.007
2.5	0.726	0.742	0.806	0.758
4.5	0.479	0.618	0.651	0.583
6.5	0.345	0.401	0.415	0.387
8.5	0.235	0.254	0.252	0.247
10.5	0.132	0.157	0.135	0.141
12.5	0.091	0.098	0.073	0.087
14.5	0.068	0.071	0.038	0.059
16.5	0.061	0.063	0.025	0.050
18.5	0.043	0.049	0.022	0.038